The Astrophysical Journal, 738:162 (16pp), 2011 September 10 doi:10.1088/0004-637X/738/2/162

PHOTOMETRIC TYPE Ia SUPERNOVA CANDIDATES FROM THE THREE-YEAR SDSS-II SN SURVEY DATA

Masao Sako[1], Bruce Bassett[2,3], Brian Connolly[1], Benjamin Dilday[4,5,6], Heather Campbell[7], Joshua A. Frieman[8,9,10], Larry Gladney[1], Richard Kessler[8,9], Hubert Lampeitl[7], John Marriner[10], Ramon Miquel[11,12], Robert C. Nichol[7], Donald P. Schneider[13], Mathew Smith[14], and Jesper Sollerman[15]

[1] Department of Physics and Astronomy, University of Pennsylvania, Philadelphia, PA 19104, USA; masao@sas.upenn.edu
[2] South African Astronomical Observatory, Observatory 7935, South Africa
[3] Department of Mathematics and Applied Mathematics, University of Cape Town, Rondebosch 7701, South Africa
[4] Las Cumbres Observatory Global Telescope Network, Goleta, CA 93117, USA
[5] Department of Physics, University of California, Santa Barbara, Broida Hall, Santa Barbara, CA 93106-9530, USA
[6] Department of Physics & Astronomy, Rutgers, the State University of New Jersey, Piscataway, NJ 08854, USA
[7] Institute of Cosmology and Gravitation, Dennis Sciama Building, University of Portsmouth, Portsmouth, PO1 3FX, UK
[8] Department of Astronomy and Astrophysics, The University of Chicago, Chicago, IL 60637, USA
[9] Kavli Institute for Cosmological Physics, The University of Chicago, Chicago, IL 60637, USA
[10] Center for Particle Astrophysics, Fermi National Accelerator Laboratory, Batavia, IL 60510, USA
[11] Institut de Física d'Altes Energies, Universitat Autónoma de Barcelona, E-08193 Barcelona, Spain
[12] Institució Catalana de Recerca i Estudis Avançats, E-08010 Barcelona, Spain
[13] Department of Astronomy & Astrophysics, The Pennsylvania State University, University Park, PA 16802, USA
[14] Astrophysics, Cosmology and Gravity Centre (ACGC), Department of Mathematics and Applied Mathematics, University of Cape Town, Rondebosch 7700, South Africa
[15] The Oskar Klein Centre, Department of Astronomy, Albaova SE-106 91 Stockholm, Sweden
Received 2011 April 13; accepted 2011 June 14; published 2011 August 22

ABSTRACT

We analyze the three-year Sloan Digital Sky Survey II (SDSS-II) Supernova (SN) Survey data and identify a sample of 1070 photometric Type Ia supernova (SN Ia) candidates based on their multiband light curve data. This sample consists of SN candidates with no spectroscopic confirmation, with a subset of 210 candidates having spectroscopic redshifts of their host galaxies measured while the remaining 860 candidates are purely photometric in their identification. We describe a method for estimating the efficiency and purity of photometric SN Ia classification when spectroscopic confirmation of only a limited sample is available, and demonstrate that SN Ia candidates from SDSS-II can be identified photometrically with ∼91% efficiency and with a contamination of ∼6%. Although this is the largest uniform sample of SN candidates to date for studying photometric identification, we find that a larger spectroscopic sample of contaminating sources is required to obtain a better characterization of the background events. A Hubble diagram using SN candidates with no spectroscopic confirmation, but with host galaxy spectroscopic redshifts, yields a distance modulus dispersion that is only ∼20%–40% larger than that of the spectroscopically confirmed SN Ia sample alone with no significant bias. A Hubble diagram with purely photometric classification and redshift-distance measurements, however, exhibits biases that require further investigation for precision cosmology.

Key words: cosmology: observations – supernovae: general – surveys

Online-only material: color figures, machine-readable tables

1. INTRODUCTION

Measurements of luminosity distances to nearby Type Ia supervovae (SNe Ia; Phillips 1993; Hamuy et al. 1996) and their distant counterparts have played a central role in modern cosmology and the remarkable discovery of an accelerating universe (Riess et al. 1998; Perlmutter et al. 1999). Many dedicated supernova (SN) surveys and follow-up programs have since then acquired light curves and spectra for several thousands of SNe in various redshift ranges: (1) at $z \lesssim 0.1$ by the Lick Observatory Supernova Search (Filippenko et al. 2001; Ganeshalingam et al. 2010), the CfA monitoring campaign (Riess et al. 1999; Jha et al. 2006a; Matheson et al. 2008; Hicken et al. 2009), SNFactory (Bailey et al. 2009), Carnegie Supernova Project Low-z Program (Contreras et al. 2010; Folatelli et al. 2010), the Palomar Transient Factory (Rau et al. 2009; Law et al. 2009), and the Panoramic Survey Telescope and Rapid Response System (Pan-STARRS[16]); (2) the SDSS-II SN Survey in the intermediate-redshift interval $0.1 \lesssim z \lesssim 0.3$ (Frieman et al. 2008; Sako et al. 2008); (3) the highest-redshift range observable from the ground at $0.3 \lesssim z \lesssim 1$ by the Supernova Legacy Survey (SNLS; Astier et al. 2006; Guy et al. 2010; Conley et al. 2011), the ESSENCE SN Survey (Miknaitis et al. 2007; Wood-Vasey et al. 2007), the Carnegie Supernova Project High-z Program (Freedman et al. 2009); and finally (4) $z \gtrsim 1$ SN Ia from space using the *Hubble Space Telescope* (Riess et al. 2004a, 2007; Dawson et al. 2009).

Many future surveys, such as the Dark Energy Survey (Flaugher et al. 2010) and the Large Synoptic Survey Telescope (LSST Science Collaborations 2009), with deeper and more wide-field imaging capabilities will probe much larger volumes of the universe allowing discoveries of thousands to tens of thousands of high-redshift SN candidates each year. Spectroscopic follow-up observations of these large, faint SN samples will require prohibitively large time allocations with existing instruments. Studies of SN properties and cosmology will, therefore, necessitate a photometric determination of the SN type,

[16] http://pan-starrs.ifa.hawaii.edu/public

cosmological redshift, and the luminosity distance from light curves with possibly a limited subsample with spectroscopic confirmation and redshift measurements.

Various methods for photometrically classifying SNe have been discussed in the literature. Optical and UV colors near maximum light, for example, have been used to distinguish SNe Ia from core-collapse SNe (Pskovskii 1977; Poznanski et al. 2002; Panagia 2003; Riess et al. 2004b; Johnson & Crotts 2006). Poznanski et al. (2007a) have developed a Bayesian method that classifies SNe using only a single epoch of photometry (see also Kuznetsova & Connolly 2007; Rodney & Tonry 2009). Template-fitting methods have been employed for spectroscopic targeting of active SN candidates (Sullivan et al. 2006; Sako et al. 2008). Sullivan et al. (2006) have performed an analysis to identify a sample of photometric SN Ia candidates from the first year of the SNLS. Dahlen et al. (2004), Poznanski et al. (2007b), Dahlen et al. (2008), Dilday et al. (2008), Dilday et al. (2010), Rodney & Tonry (2010b), and Graur et al. (2011) have also used photometric classification to measure SN rates as a function of redshift.

Although an efficient photometric SN classifier is crucial for a successful spectroscopic follow-up program and also for understanding the bias in the spectroscopic sample, the ability to estimate both the efficiency and purity of the selected sample is also important for understanding, for example, possible biases in distance measurements and studies of SN rates. Clearly, the efficiency can be improved by compromising purity, and vice versa, and the requirements may vary depending on the type of study involved.

In addition to photometrically identifying SN Ia candidates, redshifts and luminosity distances can be inferred from the same multiband light curve data. These studies of *SN cosmology without spectroscopy* have been pioneered by Barris & Tonry (2004) and carried out more recently by a number of authors. Palanque-Delabrouille et al. (2010), Kessler et al. (2010a), and Rodney & Tonry (2010a), for example, study the quality of photometric redshifts on large samples of existing data. Rodney & Tonry (2010a) also construct a photometry-only Hubble diagram of the first-year Sloan Digital Sky Survey II (SDSS-II) and SNLS spectroscopically confirmed SNe Ia using their Supernova Ontology with Fuzzy Templates method. Others show comparisons of measured and input redshifts primarily from simulations (Kim & Miquel 2007; Kunz et al. 2007; Wang et al. 2007; Wang 2007; Gong et al. 2009; Scolnic et al. 2009).

The accuracy and precision of the measured parameters depend on many observational factors including the statistical quality of the observed light curves, surface brightness of the underlying host galaxy, photometric calibration, wavelength coverage, the number of filter bandpasses, and the observing cadence. Other non-observational factors that might affect the measurements are the quality of the light curve models, assumptions on the dust properties and intrinsic SN colors, and priors used in the fits. The photometric redshift uncertainty on any individual SN is obviously larger than a typical spectroscopic redshift error, but a substantially larger number of *unbiased* redshifts and distance measurements made possible photometrically might be able to provide competitive constraints on cosmological parameters with future large-scale surveys.

Some of the existing software and algorithms, including the one presented in this paper, were recently used to participate in the Supernova Photometric Classification Challenge (Kessler et al. 2010b), a public competition for classifying SN light curves. The authors of the challenge released a large number of simulated SN light curves of undisclosed types and a small "spectroscopic" sample with known redshifts and types for training. Participants of the challenge submitted their classifications as well as photometric redshifts if available. The algorithm presented here achieved the highest overall figure of merit, although there is significant room for improvement.

This paper focuses on understanding these issues using an improved implementation of existing methods and through analysis of a much larger sample of SN candidates for testing. We use the three-year SDSS-II SN Survey data as our test bed to identify photometric SN Ia candidates with realistic estimates of sample purity. The description of the photometric classification algorithm and the spectroscopic and photometric SN samples from SDSS-II are presented in Section 2. The procedures for estimating the SN Ia typing efficiency and purity using the spectroscopic sample are described Sections 3 and 4. The properties of the photometric SN Ia candidates identified are described in Section 5. The quality of the light curve photometric redshifts is discussed in Section 6. Comparisons with simulations are shown in Section 7. Finally, our results are summarized in Section 8.

2. THE SDSS-II SN CANDIDATES

The SDSS-II SN Survey was conducted during the September–November months of 2005–2007. A 300 deg^2 region along the celestial equator was observed using the SDSS 2.5 m telescope (Gunn et al. 1998; Fukugita et al. 1996; York et al. 2000; Gunn et al. 2006) with an average cadence of four days (Frieman et al. 2008; Abazajian et al. 2009). The survey depth and area are optimal for discovering and measuring light curves of SN Ia at intermediate redshifts ($0.1 \lesssim z \lesssim 0.4$), complementing other surveys. During the search campaigns, new variable and transient sources detected in the difference images were designated as "SN candidates." After each night of imaging observations on the SDSS telescope, the SN candidates were photometrically classified based on the available multiband light curves, and a subset of the events was observed spectroscopically close to their moment of discovery (Sako et al. 2008). Photometry and results from follow-up spectroscopy from the first season are presented in Holtzman et al. (2008) and Zheng et al. (2008), respectively, and measurements of the cosmological parameters from the first-year sample and studies of the sources of systematic uncertainties are presented in Kessler et al. (2009a), Sollerman et al. (2009), and Lampeitl et al. (2010).

Over 10,000 SN candidates were discovered during the three-year SDSS-II SN Survey, and the majority of these candidates are spectroscopically unconfirmed due to limited spectroscopic resources. The goal of this paper is to photometrically identify the SN Ia candidates and to estimate the efficiency and purity of that photometric classification. We investigate whether reliable cosmological measurements can be performed from SN candidates without spectroscopic confirmation. We first describe the SN classification algorithm below and then discuss our method for estimating the efficiency and purity using a limited number of spectroscopically confirmed SNe.

2.1. Photometric SN Classification Algorithm

The candidates are classified using a light curve analysis software called "Photometric SN IDentification" (PSNID), which is an extended version of the software used for prioritizing spectroscopic follow-up observations for the SDSS-II SN Survey as

described in Sako et al. (2008).[17] Extensive tests were performed using the publicly available SNANA light curve simulations[18] as well as the data presented here. PSNID was also used to analyze simulations from the Supernova Photometric Classification Challenge and achieved the highest overall figure of merit Kessler et al. (2010b, hereafter K10b). Briefly, the software uses the observed photometry, calculates the reduced χ^2 ($\chi^2_r = \chi^2$ per degree of freedom) against a grid of SN Ia light curve models and core-collapse SN (CC SN) templates, and identifies the best-matching SN type and set of parameters with, and without, host galaxy redshift as priors in the grid search. A number of important improvements have been made, which are described below.

First, in addition to finding the light curve model with the minimum χ^2_r through a grid search, the software computes the Bayesian probabilities that a candidate could be a Type Ia, Types Ib/c, or a Type II SN. The algorithm is similar to that of Poznanski et al. (2007a) except that we subclassify CC SNe into Types Ib/c and II using an extended set of templates (see below), and also allow the SN Ia light curve shape parameter and distance modulus to vary in the fits. Specifically, we calculate the Bayesian evidence E by marginalizing the product of the likelihood function and prior probabilities over the model parameter space. For the SN Ia models, there are five model parameters—redshift z, V-band host galaxy extinction A_V, time of maximum light $T_{\rm max}$, $\Delta m_{15}(B)$ (Phillips 1993; Phillips et al. 1999), and distance modulus μ. Milky Way extinction is modeled assuming the Cardelli et al. (1989) law with $R_V = 3.1$, while extinction in the SN host galaxy assumes a total-to-selective extinction ratio of $R_V \equiv A_V/E(B-V) = 2.2$ (Kessler et al. 2009a). Priors in A_V, $T_{\rm max}$, and μ can also be applied optionally, but we set them to be flat in this present work. For the redshift, we evaluate each light curve twice using (1) a flat prior and (2) a Gaussian prior if an external redshift estimate $z_{\rm ext}$ and uncertainty σ_z are available from either the host galaxy (photometric or spectroscopic redshift) or the SN spectrum. The SN Ia Bayesian evidence is therefore

$$E_{\rm Ia} = \int_{\text{all parameters}} P(z) e^{-\chi^2/2} dz dA_V dT_{\rm max} d\Delta m_{15,B} d\mu, \quad (1)$$

where

$$P(z) = \frac{1}{\sqrt{2\pi}\sigma_z} e^{-(z-z_{\rm ext})^2/2\sigma_z^2}. \quad (2)$$

When an external redshift is not available, we assume the prior to be flat by setting $P(z) = 1$. For the SN Ib/c and SN II models, the integral over $\Delta m_{15}(B)$ is replaced with a summation over the individual templates used in the comparison:

$$E_{\rm Ibc,II} = \sum_{\text{templates}} \int P(z) e^{-\chi^2/2} dz dA_V dT_{\rm max} d\mu. \quad (3)$$

The Bayesian probability of one of the three possible SN types is then given by

$$P_{\rm type} = \frac{E_{\rm type}}{E_{\rm Ia} + E_{\rm Ibc} + E_{\rm II}}. \quad (4)$$

The probabilities $P_{\rm type}$ and minimum χ^2_r values calculated using the Gaussian spectroscopic redshift prior are denoted with a subscript z (i.e., $P_{\rm z,type}$ and $\chi^2_{z,r}$). External photometric redshifts of the host galaxies are not used in the fits in this work. The probabilities are normalized such that

$$P_{\rm Ia} + P_{\rm Ibc} + P_{\rm II} = 1, \quad (5)$$

which is equivalent to assuming that the SN candidate is a real SN and not another class of variable sources. This assumption is reasonable, since sources in Stripe 82 with a prior history of variability and other multiyear variables are rejected from our analysis (Sako et al. 2008). This set of Bayesian probabilities is useful because it quantifies the relative likelihood of SN types—the best-fit minimum χ^2_r alone is not a good indicator of the most likey SN type. As advocated by Kuznetsova & Connolly (2007), we therefore select SN Ia based on both the Bayesian probability $P_{\rm Ia}$ and the goodness-of-fit χ^2_r.

Next, although the SN Ia light curve models used herein are the same as those described in Sako et al. (2008), we have assigned empirical model errors that yield reasonable χ^2_r values for light curves with high S/N ratio. The assumed magnitude errors δm on the gri model light curves depend on the rest-frame epoch t in days from B-band maximum as follows:

$$\delta m_{\rm Ia} = \begin{cases} 0.08 + 0.04 \times (|t|/20) & |t| < 20 \text{ days}, \\ 0.12 + 0.08 \times ((|t| - 20)/60) & |t| \geqslant 20 \text{ days}. \end{cases} \quad (6)$$

The CC SN light curve templates have error in gri given by

$$\delta m_{\rm CC} = 0.08 + 0.08 \times (|t|/60) \quad (7)$$

for all epochs. The model errors in u and z are chosen to be twice the above values due to larger intrinsic model variations and calibration uncertainties in these bands. These δm parameters were determined to provide reasonable χ^2_r values ($\chi^2_r \sim 1$) primarily for nearby SN candidates with small photometric errors. They do not affect the fit results of faint candidates.

Third, we adopt CC SN light curve templates from a sample of nearby SNe discovered and observed by SDSS-II. Specifically, we use four SN Ib/c templates and four SN II templates as listed in Table 1. The SDSS-II CC SN light curve templates were generated using the Nugent et al. (2002) spectral templates, interpolating between epochs, and warping them to match each of the observed *ugriz* light curves at their respective spectroscopic redshifts. For all SNe Ib/c, we use Nugent's normal Ib/c spectral templates and we use the Type II-P templates for all SNe II. The SN II light curve photometry are available from D'Andrea et al. (2010).

The set of eight core-collapse templates listed in Table 1 were selected from a larger group of 24 templates (5 Nugent, 11 SDSS-II, and 8 from the SUSPECT[19] database) by empirically

Table 1
Core-collapse SN Templates

Type	Subtype	IAU Name	SDSS ID
Ibc	Ib	SN2005hl	2000
...	Ib	SN2005hm	2744
...	Ic	SN2006fo	13195
...	Ib	SN2006jo	14492
II	II-L/P	SN2004hx	18
...	II-P	SN2005lc	1472
...	II-P	SN2005gi	3818
...	II-P	SN2006jl	14599

[17] The software is included in the SNANA Package (Kessler et al. 2009b). A standalone version is also available directly from the author.
[18] http://sdssdp62.fnal.gov/sdsssn/SIMGEN_PUBLIC/
[19] http://bruford.nhn.ou.edu/~suspect/index1.html

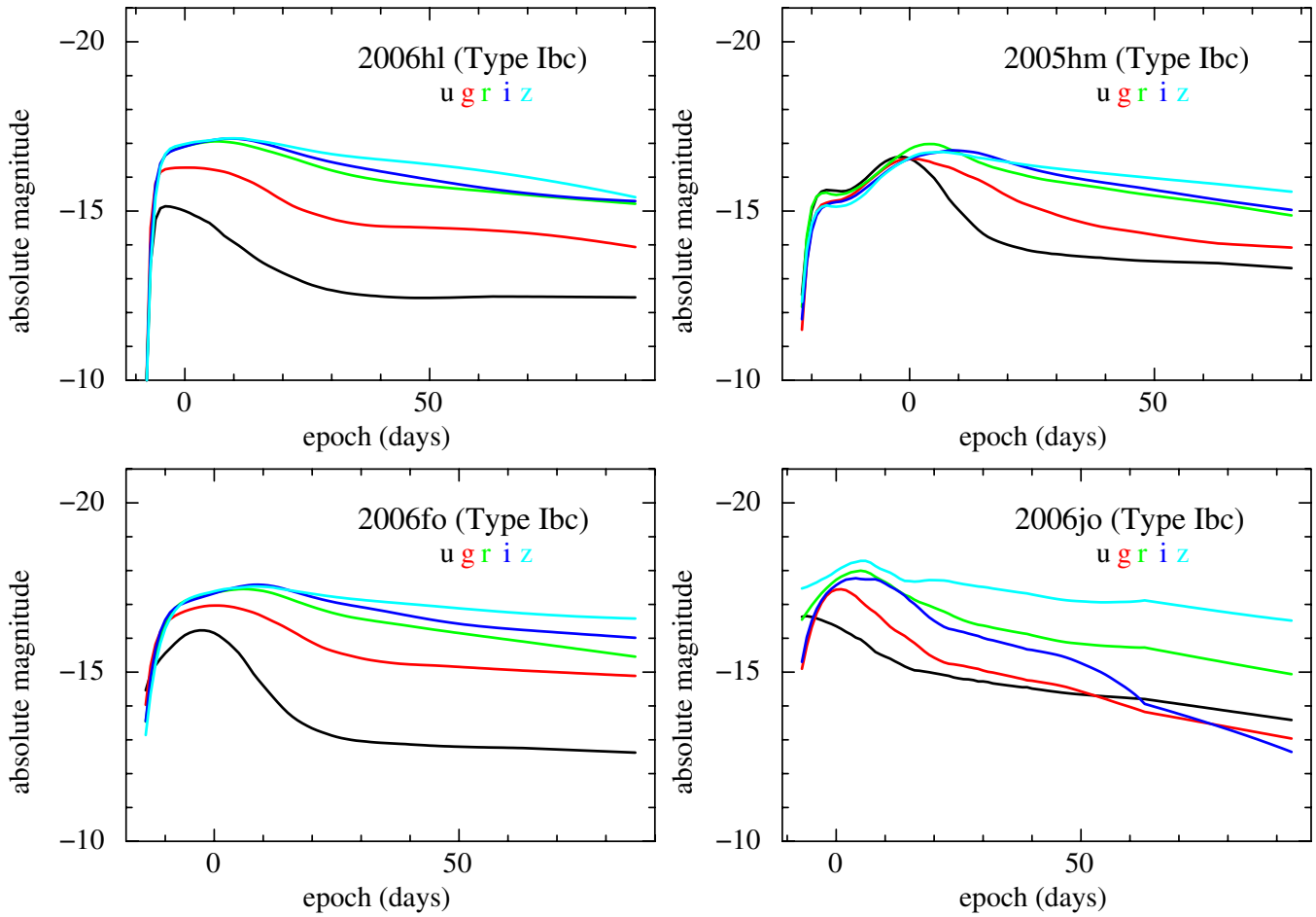

Figure 1. Absolute magnitude light curves of SN Ib/c discovered and observed by SDSS-II, which are part of the template library—SN 2005hl (top left), SN 2005hm (top right), SN 2006fo (bottom left), and SN 2006jo (bottom right).

(A color version of this figure is available in the online journal.)

maximizing the purity of the confirmed SN Ia sample. Core-collapse templates that either frequently misidentify SNe Ia as CC SNe or correctly identify only a small number of confirmed CC SNe were excluded. Rare, peculiar SNe Ia are also excluded from our template library. We also do not include templates for other types of variable sources, most notably the active galactic nuclei (AGNs), since there are other ways of rejecting the majority of these events. The rest-frame absolute magnitude *ugriz* light curves of the eight CC SNe used as templates in this analysis are shown in Figures 1 and 2.

Finally, while the Bayesian classification probabilities are computed through marginalization over the grid of the model parameters, the posterior probability distributions for each of the five parameters are estimated by running a Markov Chain Monte Carlo (MCMC). This results in a significant reduction of computing time and more reliable estimates of the parameter uncertainties, since the probability distributions are often asymmetric, show significant correlations, and can often have more than one local maximum. It is also straightforward to incorporate additional model parameters and priors.

Figure 3 shows an example output from PSNID for a spectroscopically confirmed SN Ia, 2006jz at $z = 0.20$. Derived parameter constraints from the MCMC are shown for both the flat and spectroscopic redshift priors. There are two general points that are worth noting. First, z and A_V are anti-correlated in the sense that a low-z, high-A_V SN Ia is similar to a high-z, low-A_V event. This is expected, since redshift and dust both have the effect of reddening the light curves. But since dust also attenuates the light, a larger A_V value must be compensated for by putting the event at a smaller distance modulus. This happens in the way such that z and μ, marginalized over the other three parameters, are positively correlated. The slope of this correlation is redshift-dependent. Second, the widths of the marginalized μ and A_V probability distribution function (PDF) for the flat redshift prior are only a factor $\sim$2 larger than those for a spectroscopic redshift prior. This general behavior is true for most of our well-observed SNe Ia, although the constraints using a flat-z prior degrades dramatically at higher redshifts, as shown in Figure 4 for a $z = 0.30$ confirmed SN Ia 2005it.

2.2. Confirmed and Unconfirmed Samples

We first divide the full sample of SN candidates into two groups—the spectroscopically confirmed and unconfirmed samples. The unconfirmed sample consists of sources of unknown type with no spectroscopy of the active SN candidate, but a subset of the events do have spectroscopy of their host galaxies. The spectroscopically confirmed sample consists of SNe Ia, SNe Ib/c, and SNe II as well as variable AGNs. This sample is used to study the classification criteria and also allows us to estimate the selection efficiency and purity, which is a crucial part of our analysis. The *ugriz* multiband light curves of all SN candidates

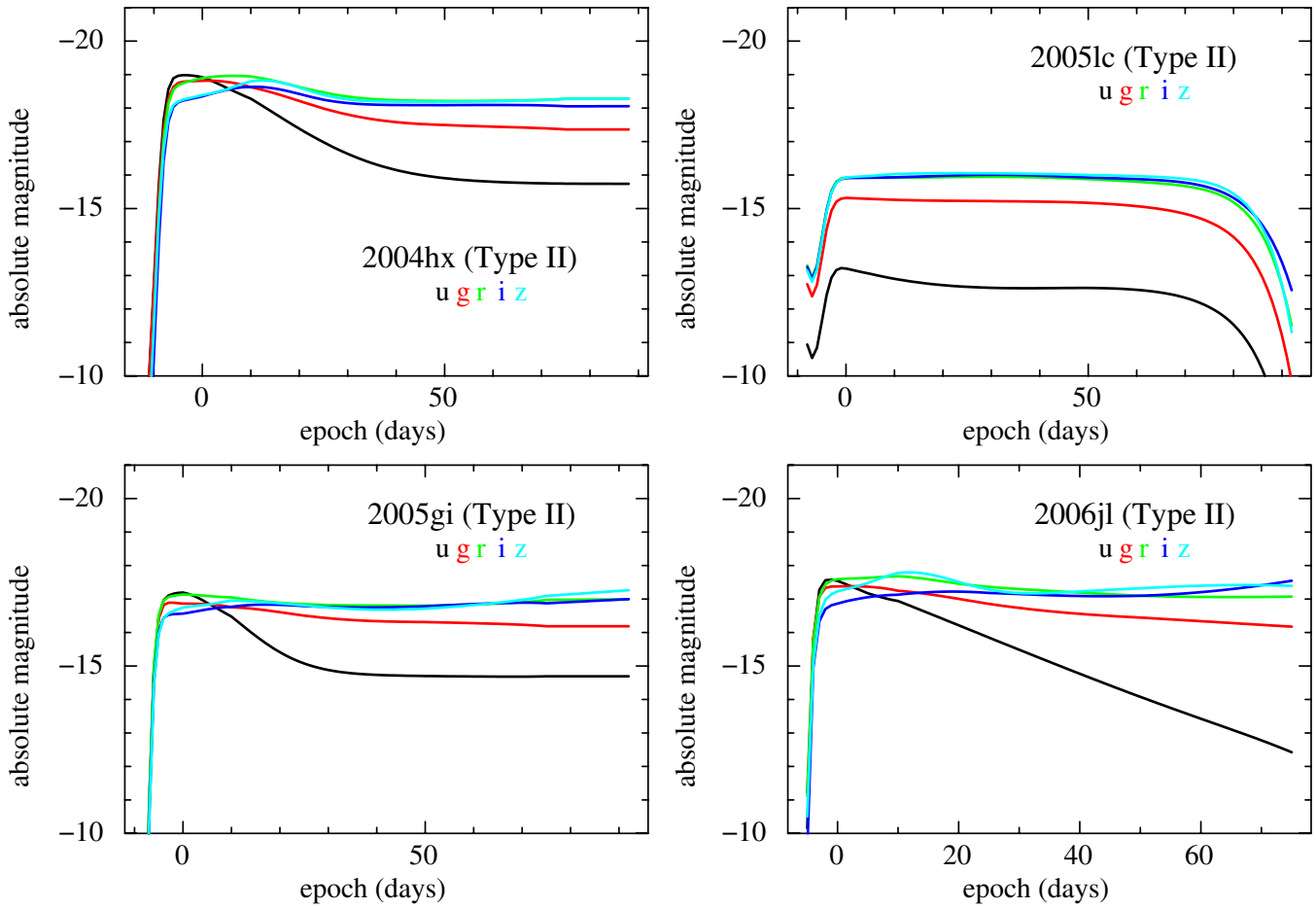

Figure 2. Absolute magnitude light curves of SN II discovered and observed by SDSS-II, which are part of the template library—SN 2004hx (top left), SN 2005lc (top right), SN 2005gi (bottom left), and SN 2006jl (bottom right).

(A color version of this figure is available in the online journal.)

are constructed using the Scene-Modeling Photometry method (Holtzman et al. 2008) and analyzed using the PSNID software described above.

The full SN sample is analyzed with PSNID, and we select the candidates that have light curve coverage and signal-to-noise ratio (S/N) that are appropriate for photometric SN Ia classification. Specifically, we consider only the candidates that meet the following three criteria: (1) have at least one epoch of photometry near peak at $-5 < t < +5$ days in the SN rest frame and at least one additional epoch after peak at $t > +15$ days, which are determined from the best-fit SN Ia model, irrespective of whether or not the fit is acceptable; (2) have maximum S/N greater than five in at least two of the *gri* bands; and (3) were detected during only one search season. These cuts are referred to as the light curve quality cuts.

The spectroscopically confirmed sample consists of 508 SNe Ia, 80 CC SNe (18 SNe Ib/c, 62 SNe II), and 202 AGNs.[20] We refer to these as the "conf-Ia," "conf-CC," and the "conf-AGN" samples. After imposing the light curve quality cuts, this sample is reduced to 367 SNe Ia, 45 CC SNe, and 83 AGNs, for a total of 495 events when a flat spectroscopic redshift prior is used. Using the spectroscopic redshift prior results in 551 events. The numbers differ since the two forms of the redshift priors can result in best-fit SN Ia models with dramatically different dates of maximum light, especially for the AGN.

There is a significant bias in the spectroscopically confirmed SN sample toward brighter events. For the SDSS-II SN Survey, our primary goal was to discover and study the properties of SNe Ia, so only a small fraction of CC SN candidates were observed for spectroscopy. A detailed study of the impact on photometric SN Ia typing due to contaminating sources is, therefore, limited by this small number of spectroscopically confirmed CC SNe.

To help quantify this bias, we identified the SN candidates that are associated with galaxies with spectra from the SDSS spectroscopic survey (Eisenstein et al. 2001; Strauss et al. 2002; Richards et al. 2002). These galaxies have well-defined selection criteria and, as we describe below, will help quantify the spectroscopic targeting bias and to obtain a better estimate of the level of contamination from non-SN Ia events. There are a total of 2369 SN candidates that are within 10″ from an SDSS spectroscopic galaxy. This sample is referred to as the "$z_{\rm SDSS}$" sample. After light curve quality cuts, there are 448 and 499 sources for the flat and spectroscopic redshift priors, respectively, which include both confirmed and unconfirmed SN candidates. The majority of the sources are rejected because of their multiyear variability, suggesting that these sources are likely variable AGNs whose nuclear activity is not immediately apparent from their optical spectra. The samples are summarized in Table 2. The redshift distributions of the four different spectroscopic samples are shown in Figure 5.

[20] Of the 202 AGNs, 58 are in the DR7 spectroscopic quasar catalog from Schneider et al. (2010).

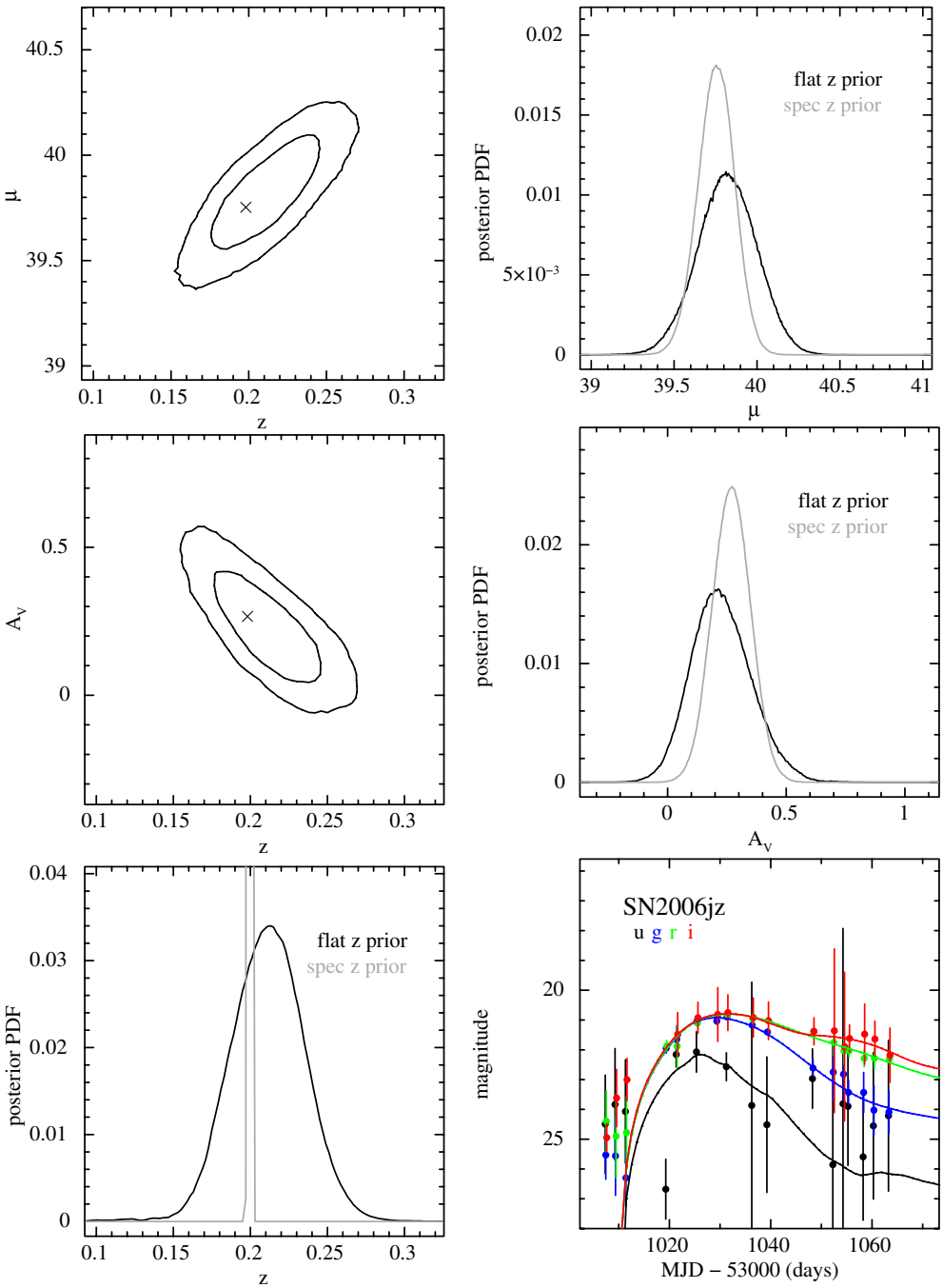

Figure 3. Example of the posterior PDFs for a spectroscopically confirmed SN Ia 2006jz at $z = 0.20$. The observed $ugri$ light curves and the best-fit SN Ia model are shown on the bottom right panel. The top left and middle left panels show 1σ and 2σ contours in the z–μ and z–A_V planes, respectively, assuming a flat redshift prior. The "×'s" indicates the median parameter values when a spectroscopic-redshift prior is used. The two panels on the right and the bottom left panel show the posterior PDF in μ, A_V, and z marginalized over the other four parameters using the flat (black) and spectroscopic (gray) redshift priors.

(A color version of this figure is available in the online journal.)

The unconfirmed sample consists of a total of 3221 candidates that pass the same light curve quality cuts. Of these 3221 candidates, 2776 have no spectroscopic observations, while the remaining 445 candidates are either part of the $z_{\rm SDSS}$ sample described above (230 candidates) or have host galaxy redshifts from our own follow-up observations (215 candidates).

A histogram of the maximum r-band S/N of this sample is shown in Figure 6. The mean S/N of ∼30 for the spectroscopic sample is substantially higher than that of the photometric sample, which has a mean S/N of ∼10. The implications of this difference are discussed in Section 8.

3. SN CLASSIFICATION FIGURE OF MERIT

Since our goal here is to identify SNe Ia, we define the photometric typing efficiency $\epsilon_{\rm Ia}$ as the fraction of SNe Ia, after software S/N light curve quality cuts, that are photometrically identified as SNe Ia. Let $\mathcal{N}_{\rm Ia}^{\rm true}$ be the number of true SNe Ia photometrically identified as SNe Ia and $\mathcal{N}_{\rm Ia}^{\rm CUT}$ be the total number of SNe Ia in the sample after the light curve quality cuts, we define the photometric SN Ia selection efficiency to be

$$\epsilon_{\rm Ia} = \frac{\mathcal{N}_{\rm Ia}^{\rm true}}{\mathcal{N}_{\rm Ia}^{\rm CUT}}. \quad (8)$$

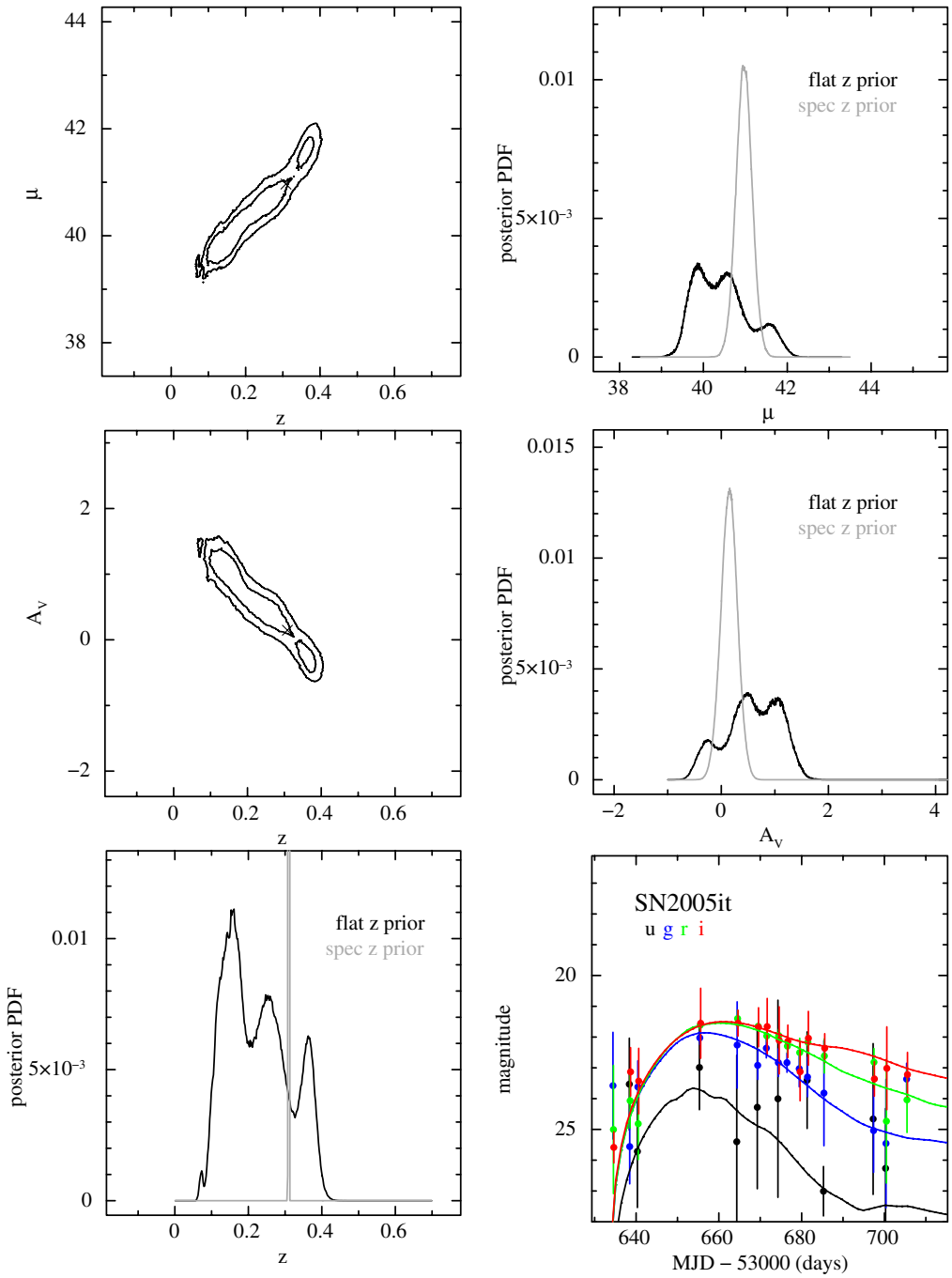

Figure 4. Same as in Figure 3 for a spectroscopically confirmed SN Ia 2005it at $z = 0.30$.
(A color version of this figure is available in the online journal.)

Note that this is not the true SN Ia identification efficiency since the denominator $\mathcal{N}_{\rm Ia}^{\rm CUT}$ includes only the events that pass the S/N and light curve quality cuts. In terms of the total number of SNe Ia ($\mathcal{N}_{\rm Ia}^{\rm TOT}$) that were detected in the area observed by the survey,

$$\mathcal{N}_{\rm Ia}^{\rm CUT} = \epsilon_{\rm CUT} \mathcal{N}_{\rm Ia}^{\rm TOT}, \quad (9)$$

where $\epsilon_{\rm CUT}$ is, in general, a function of z, A_V, $\Delta m_{15}(B)$, peak magnitude, time of maximum light, software detection threshold, requirements on light curve S/N and temporal coverage, and the observing conditions. The determination of the value of $\epsilon_{\rm CUT}$ is beyond the scope of the paper, but the effect of our selection cuts can be modeled using the SNANA Package.

Adopting the convention similar to that used in evaluating the SN Photometric Classification Challenge (hereafter SNPhotCC; K10b); we define the *photometric purity* $\eta_{\rm Ia}$ as the fraction of the candidates identified as SNe Ia that are actual SNe Ia with a penalty factor $\mathcal{W}_{\rm Ia}^{\rm false}$ described below. Let $\mathcal{N}_{\rm Ia}^{\rm false}$ be the number of non-SNe Ia incorrectly identified as SNe Ia, the photometric purity of the sample is

$$\eta_{\rm Ia} = \frac{\mathcal{N}_{\rm Ia}^{\rm true}}{\mathcal{N}_{\rm Ia}^{\rm true} + \sum_i \mathcal{W}_{\rm Ia,i}^{\rm false} \mathcal{N}_{\rm Ia,i}^{\rm false}}, \quad (10)$$

where the sum in the denominator allows for several classes i of contaminating sources (e.g., CC SNe, AGNs, and variable

Table 2
The SDSS-II Spectroscopic Sample

Type	Total	Flat Redshift Prior			Spectroscopic Redshift Prior		
		Good[a]	$P_{\rm Ia} \geqslant 0.9$	$P_{\rm Ia} \leqslant 0.1$	Good[a]	$P_{\rm Ia} \geqslant 0.9$	$P_{\rm Ia} \leqslant 0.1$
Confirmed SN Ia	508	367	357	2	371	366	1
Confirmed CC SN	80	45	14	30	45	11	32
Confirmed AGN	202	83	32	44	135	86	46
SN with $z_{\rm SDSS}$	2369	448	248	159	499	317	150
Total	3159	732	539	201	788	599	163

Note.
[a] This sample includes SNe that satisfy the following photometric quality criteria: (1) there is at least one epoch of photometry at $-5 < t < +5$ days from peak and another epoch at $+5 < t < +15$ days from peak for the best-fit SN Ia model, (2) there is at least two filter measurements with S/N > 5, and (3) the candidate was detected in only a single search season.

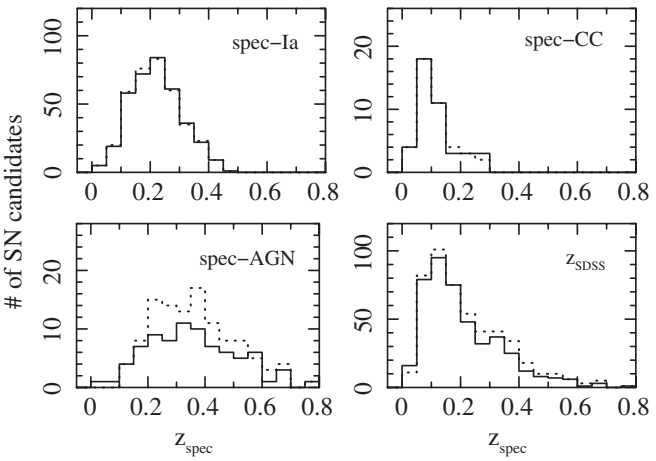

Figure 5. Redshift distributions of the conf-Ia (top left), conf-CC (top right), conf-AGN (bottom left), and $z_{\rm SDSS}$ (bottom right) samples used in our studies (see Section 2.2 for descriptions). The solid and dashed histograms represent the samples that pass our light curve quality cuts with the flat and spectroscopic redshift priors, respectively. The redshift bins are $\Delta z = 0.05$ wide.

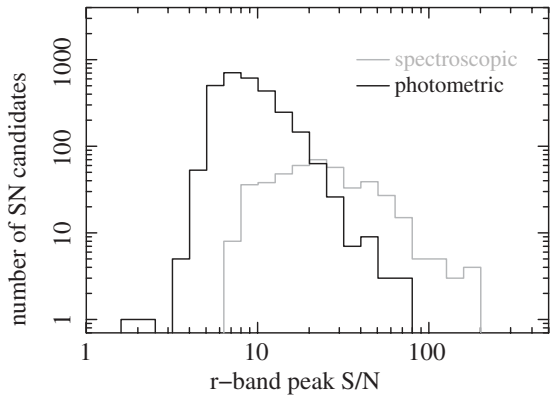

Figure 6. Distributions of maximum *r*-band S/N of the spectroscopically confirmed SN candidates (dashed) and photometric candidates (solid) considered in this work. The spectroscopic sample has an average peak S/N of ∼30 while the photometric sample has average S/N of ∼10.

stars) possibly with different penalty factors. We define a figure of merit ($\mathcal{C}_{\rm FoM\text{-}Ia}$) as

$$\mathcal{C}_{\rm FoM\text{-}Ia} = \epsilon_{\rm Ia} \times \eta_{\rm Ia}. \quad (11)$$

This definition of $\mathcal{C}_{\rm FoM\text{-}Ia}$ is designed for real data and differs from the *pseudo-purity* from the SNPhotCC by the unknown factor $1/\epsilon_{\rm CUT}$, i.e., $\mathcal{C}_{\rm FoM\text{-}Ia} = \mathcal{C}^{\rm SNPhotCC}_{\rm FoM\text{-}Ia}/\epsilon_{\rm CUT}$. K10b also define the *true purity* to be the case for $\mathcal{W}^{\rm false}_{\rm Ia} = 1$. This figure of merit is only one measure of success, and it is not necessarily the optimal measure for all types of studies. Higher SN Ia purity might be more important than efficiency for certain studies and vice versa. Finally, we define the *contamination* $\kappa_{\rm Ia}$ as

$$\kappa_{\rm Ia} = 1 - \eta_{\rm Ia}. \quad (12)$$

These quantities determined with the spectroscopic redshift prior are designated with a subscript z.

To give a simple numerical example, consider a survey that is capable of detecting 100 SNe Ia that pass S/N and light curve quality cuts. A photometric classifier that identifies 90 candidates as SNe Ia, of which 10 are actually non-Ia events has an efficiency of $\epsilon_{\rm Ia} = 80/100 = 0.80$, purity of $\eta_{\rm Ia} = 80/90 = 0.89$, and contamination of $\kappa_{\rm Ia} = 1–0.89 = 0.11$. In practice, however, these quantities can be determined only for the spectroscopically confirmed SN sample for which the correct type is known. The efficiency, purity, or some combination of these two parameters can be optimized by choosing the appropriate values for $P_{\rm Ia}$ and χ^2_r. If the spectroscopic sample is an unbiased representation of all of the SN candidates, then one can expect the efficiency and the purity of both the spectroscopic and photometric samples to be the same within statistical uncertainties. However, this is almost never the case in a blind SN survey given limited spectroscopic resources. SN candidates that are brighter and/or suffer less host galaxy contamination will have higher spectroscopic success and completeness. This is illustrated in Figure 6, which shows that the light curve peak S/N of the spectroscopic sample is on average a factor of ∼3 higher than that of the photometric sample. Below we describe a method to correct for this bias and to estimate the efficiency and purity of the photometric sample using a limited and biased spectroscopic training set.

4. ESTIMATING THE EFFICIENCY AND PURITY

4.1. SN Ia Identification with Spectroscopic Redshifts

We first estimate the efficiency and purity of photometric SN Ia identification when spectroscopic redshifts are used as priors in the light curve fits. We determine $\mathcal{N}^{\rm true}_{z,{\rm Ia}}$ and $\mathcal{N}^{\rm false}_{z,{\rm Ia}}$ from the spectroscopic SN Ia and CC SN and how they depend on the minimum $P_{z,{\rm Ia}}$ and the maximum allowed $\chi^2_{z,r}$. This is relevant for future SN surveys that will, for example, obtain spectra of all SN candidate host galaxies after the search, but not spectra of all the active SN candidates. The values for $P_{z,{\rm Ia}}$ and $\chi^2_{z,r}$ are shown

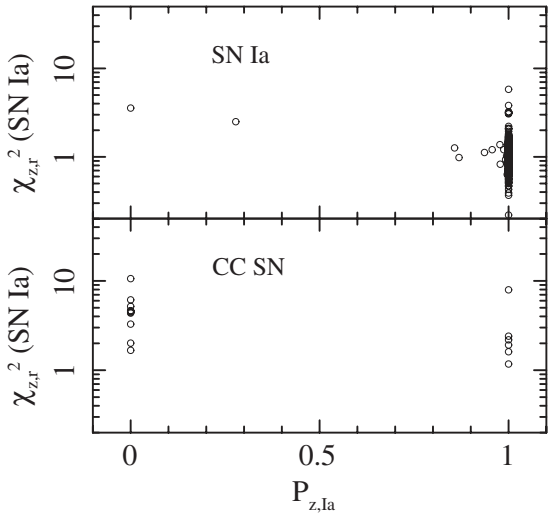

Figure 7. Distribution of $P_{z,\mathrm{Ia}}$ and $\chi^2_{z,r}$ values for the spectroscopically confirmed SNe Ia (top panel) and CC SNe. Spectroscopic redshifts are used as priors in all of the fits.

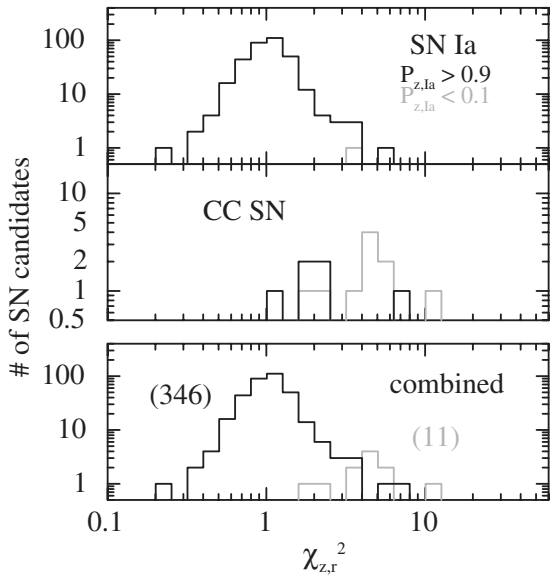

Figure 8. Histograms of best-fit $\chi^2_{z,r}$ values for an SN Ia model for $P_{\mathrm{Ia}} \geqslant 0.9$ (black) and $P_{\mathrm{Ia}} \leqslant 0.1$ (gray) for the spectroscopically confirmed SNe Ia (top panel) and CC SNe (bottom panel).

in Figure 7 separately for the spectroscopically confirmed SN Ia and CC SN samples.

As shown in the top panel of Figure 7, all but a handful of SNe Ia are well fit to an SN Ia model. Of the $\mathcal{N}^{\mathrm{CUT}}_{\mathrm{z,Ia}} = 371$ spectroscopic SNe Ia that pass the light curve quality cuts, 366 sources have $P_{z,\mathrm{Ia}} \geqslant 0.9$. Only a single SN Ia (SN 2007qd; McClelland et al. 2010) has $P_{z,\mathrm{Ia}} \leqslant 0.1$. This event is a nearby peculiar 2002cx-like event, which is underluminous compared to normal SNe Ia and has an extremely low expansion velocity (Li et al. 2003; Jha et al. 2006b). There are other nearby peculiar SNe Ia in our sample (SN 2005hk, Phillips et al. 2007; SN 2005gj, Aldering et al. 2006; Prieto et al. 2007), but these candidates were detected over two search seasons due to their brightness and slow decline, and were, therefore, rejected. The bottom panel of the same figure, however, shows that a substantial fraction of the spectroscopic CC SNe also satisfy $P_{z,\mathrm{Ia}} \geqslant 0.9$ implying that the contamination can be significant depending on the maximum allowed $\chi^2_{z,r}$ value used for the SN Ia identification. Specifically, 11 out of the 45 CC SNe (24%) that satisfy our light curve quality cuts have $P_{z,\mathrm{Ia}} \geqslant 0.9$. If no other cuts are invoked, then $\mathcal{N}^{\mathrm{true}}_{\mathrm{z,Ia}} = 366$ and $\mathcal{N}^{\mathrm{false}}_{\mathrm{z,Ia}} = 11$. We also note that the majority of the sources have either $P_{z,\mathrm{Ia}} \sim 0$ or $P_{z,\mathrm{Ia}} \sim 1$, so both $\mathcal{N}^{\mathrm{true}}_{\mathrm{z,Ia}}$ and $\mathcal{N}^{\mathrm{false}}_{\mathrm{z,Ia}}$ are not sensitive to the precise choice of the minimum $P_{z,\mathrm{Ia}}$.

Before determining how $\mathcal{N}^{\mathrm{true}}_{\mathrm{z,Ia}}$ and $\mathcal{N}^{\mathrm{false}}_{\mathrm{z,Ia}}$ depend on the choice of the maximum $\chi^2_{z,r}$, we note that 5 of the 11 CC SNe with $P_{z,\mathrm{Ia}} \geqslant 0.9$ can be rejected by requiring the light curve photo-z (z_{lc}), using a flat redshift prior, to be within 3σ of the spectroscopic redshift z_{spec}; i.e., $|z_{\mathrm{lc}} - z_{\mathrm{spec}}|/\sigma_z < 3$. We reject candidates that fail this cut and show the distributions of the $\chi^2_{z,r}$ values for the SNe Ia and CC SNe in Figure 8 for $P_{z,\mathrm{Ia}} \geqslant 0.9$ and $P_{z,\mathrm{Ia}} \leqslant 0.1$. Of the 366 SNe Ia and 11 CC SNe with good light curves and $P_{z,\mathrm{Ia}} \geqslant 0.9$, 22, and 5 candidates, respectively, are rejected by this requirement on redshift agreement. Therefore, there are only six CC SNe that satisfy all SN Ia selection cuts.

In the last step, we estimate the unknown factor $\mathcal{W}^{\mathrm{false}}_{\mathrm{z,Ia}}$, which can be interpreted as a penalty factor for spectroscopic incompleteness and targeting biases. The SDSS-II SN Survey follow-up strategy was to observe the "good" SN Ia candidates at higher priority than the CC SN candidates, especially for the fainter ($r \gtrsim 20.5$ mag) sources due to limited spectroscopic resources. A simple interpretation of this factor is that if our follow-up strategy had instead been to observe a random sample of SN candidates, then we would have spectroscopically identified $\mathcal{W}^{\mathrm{false}}_{\mathrm{z,Ia}}$ times more CC SNe.

One way to estimate this bias factor is to select a subsample of SN candidates with spectroscopic redshifts, which is representative of the underlying distribution of the SN types. The ratio of these candidates with $P_{z,\mathrm{Ia}} \leqslant 0.1$ to those with $P_{z,\mathrm{Ia}} \geqslant 0.9$ can then be interpreted to be approximately the ratio of CC SNe to SNe Ia in our survey.

This can be done by considering the SN candidates in galaxies with redshifts from the SDSS spectroscopic survey, which has a set of well-defined selection criteria. We identify candidates in the main galaxy (Strauss et al. 2002), quasar (Richards et al. 2002), and the Luminous Red Galaxy (LRG; Eisenstein et al. 2001) samples. The LRG sample is several magnitudes deeper than the main galaxy sample and consists primarily of passive galaxies with old stellar populations, which do not host any CC SNe. We include this sample to account for the fact that SNe Ia are also on average a few magnitudes more luminous than CC SNe, so a magnitude-limited survey will discover many more SNe Ia than CC SNe. The distributions of $\chi^2_{z,r}$ for $P_{z,\mathrm{Ia}} \geqslant 0.9$ and $P_{z,\mathrm{Ia}} \leqslant 0.1$ for candidates in the SDSS galaxy spectroscopy sample with $|z_{\mathrm{lc}} - z_{\mathrm{spec}}|/\sigma_z < 3$ are shown in Figure 9. The ratio of the number of candidates with $P_{z,\mathrm{Ia}} \geqslant 0.9$ to those with $P_{z,\mathrm{Ia}} \leqslant 0.1$ is $197/56 = 3.5$ compared to $350/11 = 32$ for the combined spectroscopic sample shown in the bottom panel of Figure 8. The bias (penalty) factor for the spectroscopic sample can, therefore, be estimated to be $\mathcal{W}^{\mathrm{false}}_{\mathrm{z,Ia}} = 32/3.5 = 9.0$. An unbiased spectroscopic follow-up strategy would have resulted in $\mathcal{W}^{\mathrm{false}}_{\mathrm{z,Ia}} = 9.0$ times more contaminating CC SNe for SN Ia identification.

We use this penalty factor to calculate $\epsilon_{\mathrm{z,Ia}}$ and $\eta_{\mathrm{z,Ia}}$ as functions of the maximum $\chi^2_{z,r}$. The expression for the purity is

$$\eta_{\mathrm{z,Ia}} = \frac{\mathcal{N}^{\mathrm{true}}_{\mathrm{z,Ia}}}{\mathcal{N}^{\mathrm{true}}_{\mathrm{z,Ia}} + \mathcal{W}^{\mathrm{false}}_{\mathrm{z,Ia}} \mathcal{N}^{\mathrm{false}}_{\mathrm{z,Ia}}}. \quad (13)$$

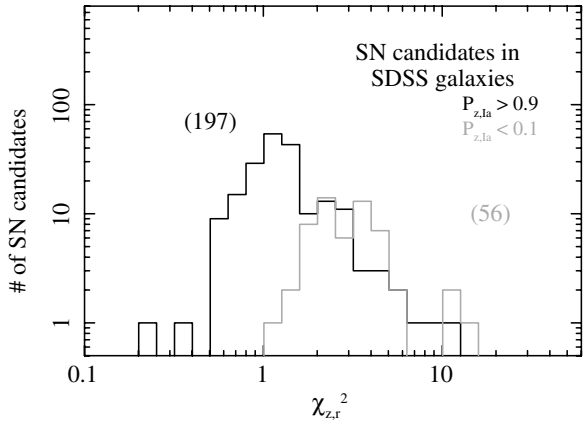

Figure 9. Histograms of best-fit χ_r^2 values for an SN Ia model for $P_{z,\mathrm{Ia}} \geqslant 0.9$ (black) and $P_{z,\mathrm{Ia}} \leqslant 0.1$ (gray) for the SN candidates in SDSS spectroscopic galaxies using the redshift as a prior.

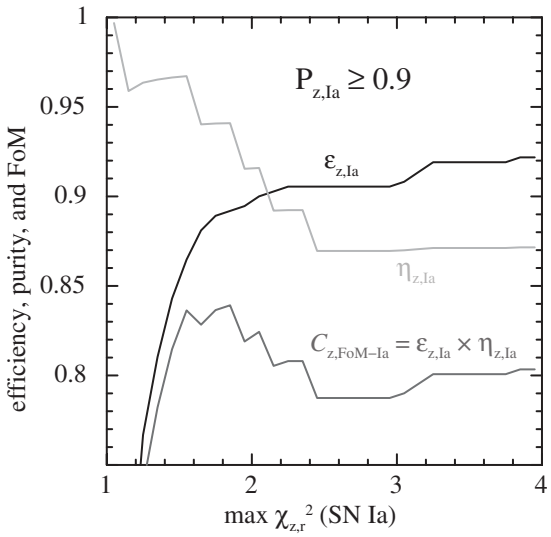

Figure 10. Efficiency, purity, and figure of merit for the spectroscopically confirmed SN as functions of the maximum-allowed $\chi_{z,r}^2$ for $P_{z,\mathrm{Ia}} \geqslant 0.9$.

Figure 10 shows how $\epsilon_{z,\mathrm{Ia}}$, $\eta_{z,\mathrm{Ia}}$, and $\mathcal{C}_{z,\mathrm{FoM\text{-}Ia}}$ depend on the maximum-allowed $\chi_{z,r}^2$ for $P_{z,\mathrm{Ia}} \geqslant 0.9$. The figure of merit has a broad maximum value of $\mathcal{C}_{z,\mathrm{FoM\text{-}Ia}} \sim 0.84$ at approximately $\chi_{z,r}^2 = 1.8$, where the efficiency and purity are ∼89% and ∼94%, respectively. A caveat to the estimate of $\eta_{z,\mathrm{Ia}}$ is that it is based on only six confirmed CC SNe that pass our SN Ia selection cuts.

4.2. SN Ia Identification without Spectroscopic Redshifts

We next determine $\mathcal{N}_{\mathrm{Ia}}^{\mathrm{true}}$ and $\mathcal{N}_{\mathrm{Ia}}^{\mathrm{false}}$ when no external redshift information is available to provide additional constraints in the light curve fits. Here we have an additional source of contaminating sources—variable AGNs—which can be identified if either the galaxy spectrum is available or the candidate is variable over a long period of time ($\gtrsim$ 1 year). We use the confirmed SN and the AGN samples discussed in Section 2.2 to determine how the efficiency, purity, and figure of merit depend on the minimum P_{Ia} and the maximum allowed χ_r^2 using the flat redshift prior. The three panels in Figure 11 show the P_{Ia} and χ_r^2 values for the spectroscopic SN Ia, CC SN, and AGN samples. As with the previous case, most of the spectroscopic SNe Ia are clustered near $P_{\mathrm{Ia}} \sim 1$ and $\chi_r^2 \sim 1$, indicating that

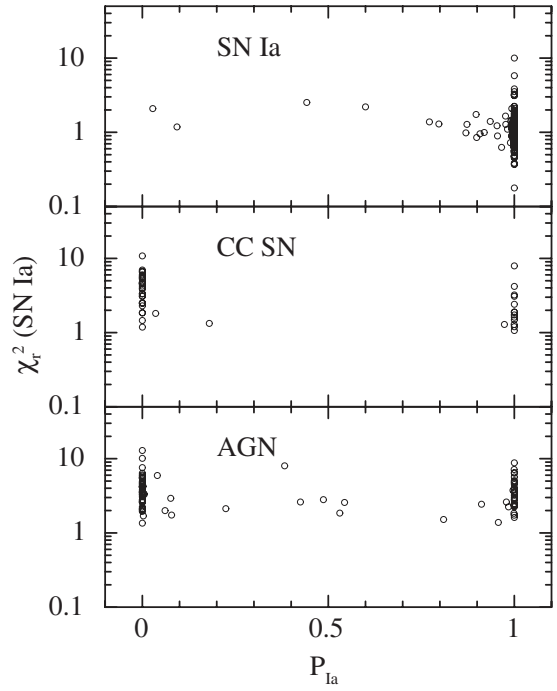

Figure 11. Distributions of P_{Ia} and χ_r^2 values for the spectroscopically confirmed SNe Ia (top panel), CC SNe (middle panel), and AGNs (bottom panel). The fits were performed with a flat redshift prior.

they are well fit to SN Ia models. There are also a handful of CC SNe and AGNs with $P_{\mathrm{Ia}} \sim 1$, however, so the amount of contamination can again be substantial depending on the maximum allowed χ_r^2.

We also show in Figure 12 histograms of the χ_r^2 values for the same sources for $P_{\mathrm{Ia}} \geqslant 0.9$. Of the $\mathcal{N}_{\mathrm{Ia}}^{\mathrm{CUT}} = 367$ spectroscopic SNe Ia that pass our light curve quality cuts, 357 sources have $P_{\mathrm{Ia}} \geqslant 0.9$. There are also 14 CC SNe and 32 AGNs with $P_{\mathrm{Ia}} \geqslant 0.9$.

For estimating η_{Ia}, we apply the penalty factor only on the CC SN sample where the bias is more significant. Almost all of the spectroscopic AGN confirmation came from SDSS quasar spectroscopy (Richards et al. 2002) and not from our own targeting, so we assume that this sample is unbiased. The expression for the efficiency is given in Equation (8). We write the purity explicitly as

$$\eta_{\mathrm{Ia}} = \frac{\mathcal{N}_{\mathrm{Ia}}^{\mathrm{true}}}{\mathcal{N}_{\mathrm{Ia}}^{\mathrm{true}} + \mathcal{W}_{\mathrm{Ia,CC}}^{\mathrm{false}} \mathcal{N}_{\mathrm{Ia,CC}}^{\mathrm{false}} + \mathcal{N}_{\mathrm{Ia,AGN}}^{\mathrm{false}}}, \qquad (14)$$

where we have assumed $\mathcal{W}_{\mathrm{Ia,AGN}}^{\mathrm{false}} = 1$. The penalty factor $\mathcal{W}_{\mathrm{Ia,CC}}^{\mathrm{false}}$ can be estimated from the histograms shown in the bottom panel of Figures 12 and 13. Specifically, we have $\mathcal{W}_{\mathrm{Ia,CC}}^{\mathrm{false}} = (403/76)/(259/199) = 4.1$ using the same method as for the case with the spectroscopic redshift prior. We show in Figure 14 the efficiency and purity as a function of the maximum-allowed χ_r^2 value. Also shown is the figure of merit, which exhibits a broad maximum at $\mathcal{C}_{\mathrm{FoM\text{-}Ia}} = 0.86$. At $\chi_r^2 \sim 1.6$, the efficiency and purity are ∼92% and ∼94%, respectively.

5. SDSS-II PHOTOMETRIC SN Ia CANDIDATES

We now evaluate the light curves of the 445 candidates with spectroscopic redshift measurements of their host galaxies. Their SN types are unknown because there were no spectroscopic observations of these objects. Selection with $P_{z,\mathrm{Ia}} \geqslant 0.90$,

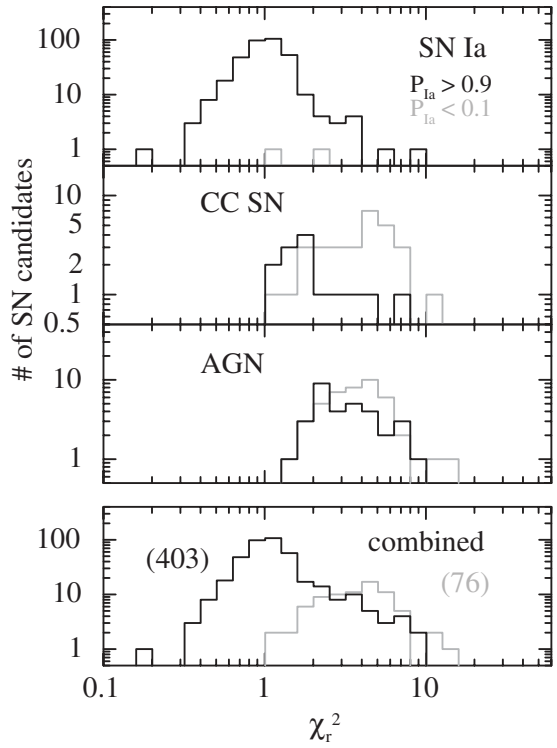

Figure 12. Histograms of best-fit χ^2_r values for an SN Ia model for $P_{\rm Ia} \geqslant 0.9$ (black) and $P_{\rm Ia} \leqslant 0.1$ (gray) for the spectroscopically confirmed (from top to bottom) (1) SNe Ia, (2) CC SNe, (3) AGNs, and (4) all three samples combined. Note that the vast majority of SNe Ia have $P_{\rm Ia} \geqslant 0.9$. The contaminating false positives are the CC SNe and AGNs represented by the black histograms with $P_{\rm Ia} \geqslant 0.9$, and there are only a small number of those sources in our sample.

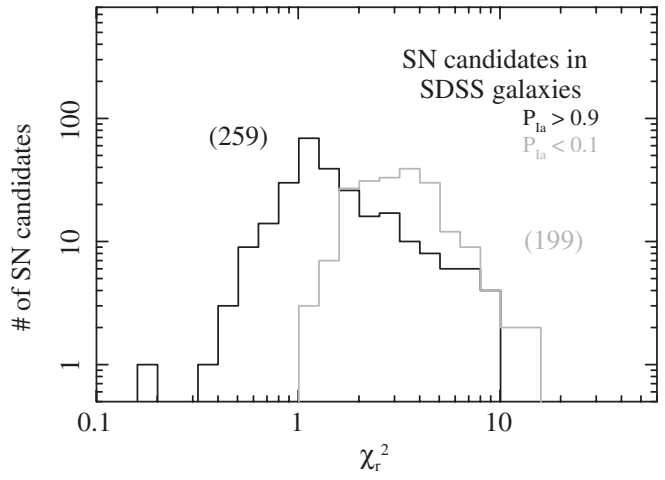

Figure 13. Histograms of best-fit χ^2_r values for an SN Ia model for $P_{\rm Ia} \geqslant 0.9$ (black) and $P_{\rm Ia} \leqslant 0.1$ (gray) for the SN candidates in SDSS spectroscopic galaxies.

$\chi^2_{z,r} \leqslant 1.8$, and $|z_{\rm lc} - z_{\rm spec}|/\sigma_z < 3$ results in 210 candidates shown in Figure 15. Based on the analysis presented in Section 4.1, we expect this sample to have an efficiency of ∼89%, purity of ∼94%, and a figure of merit of ∼0.84. We refer to this sample of 210 candidates as the "$z_{\rm host}$-Ia sample." Their candidate ID, coordinates, spectroscopic redshifts, and light curve fit results are listed in Table 3.

From the 2776 candidates with no spectroscopy, identifying sources with $P_{\rm Ia} \geqslant 0.90$ and $\chi^2_r \leqslant 1.6$ results in 860 purely photometric SN Ia candidates, which we refer to as the "photo-Ia sample." The selection is shown in Figure 16. We expect this sample to have an efficiency of ∼92%, a purity of ∼94%, and a figure of merit of 0.86. Its redshift distribution is shown in Figure 17. The mean redshift of the photo-Ia sample is $\bar{z} = 0.31$ compared to $\bar{z} = 0.22$ for the spectroscopically confirmed sample. The full list of candidates is provided in Table 4. In addition to their coordinates, we provide the photometric light curve redshifts $z_{\rm lc}$ marginalized over all the other parameters. The reliability of these values is discussed in the following section.

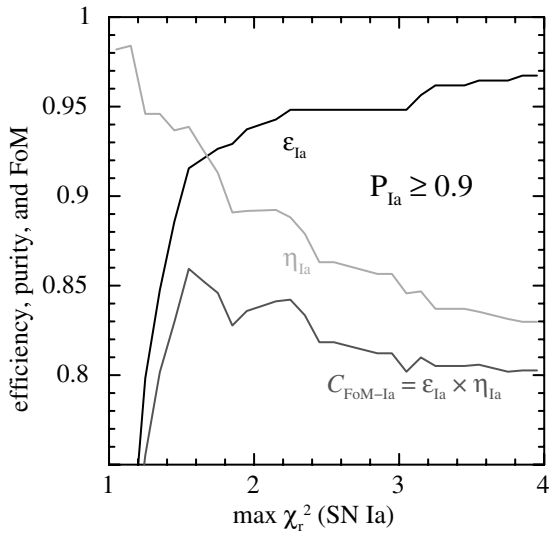

Figure 14. Efficiency, purity, and figure of merit for the spectroscopically confirmed SN as functions of the maximum-allowed χ^2_r for $P_{\rm Ia} \geqslant 0.9$.

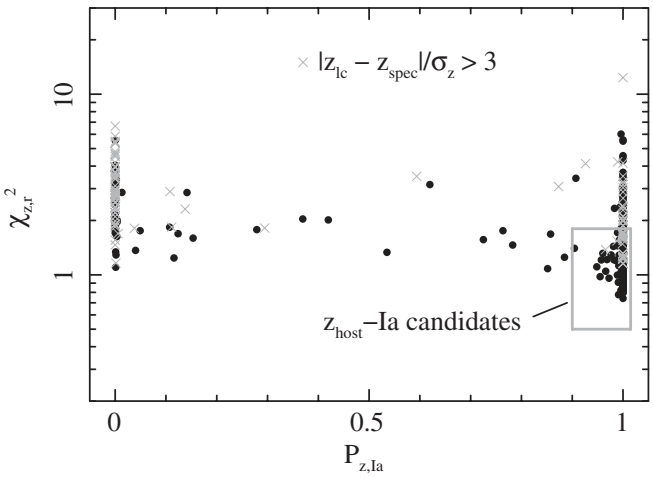

Figure 15. $P_{z,\rm Ia}$ vs. $\chi^2_{z,r}$ for the 445 photometric candidates with galaxy spectroscopic redshifts. Candidates that do not meet the light curve photo-z cut ($|z_{\rm lc} - z_{\rm spec}|/\sigma_z < 3$) are shown as crosses. The 210 $z_{\rm host}$-Ia candidates identified are bounded by the red box shown in the lower right.

The light curves of these candidates, as well as all of the other SN candidates, will be made available soon as part of the SDSS-II SN Survey Data Release.

6. PHOTOMETRIC REDSHIFTS AND DISTANCES

The light curve redshifts $z_{\rm lc}$ are determined by marginalizing over the other four model parameters: A_V, $T_{\rm max}$, $\Delta m_{15}(B)$, and μ. For each SN candidate, the posterior PDF is constructed from the MCMC output. The redshifts listed in Table 4 correspond to the median $z_{\rm lc}$ and the $\pm 34.1\%$ (1σ) upper and lower limits.

Table 3
SDSS-II $z_{\rm host}$–Ia Candidates

SDSS ID[a]	R.A.[b]	Decl.[b]	$z_{\rm spec}$	A_V	Δm_{15} (B)	$P_{z,\rm Ia}$	$\chi^2_{z,r}$
703	−23.782080	+0.650725	0.3000 ± 0.0100	$0.04^{+0.16}_{-0.18}$	$0.70^{+0.13}_{-0.08}$	1.000	0.99
779	26.673738	−1.020580	0.2377 ± 0.0005	$0.21^{+0.13}_{-0.13}$	$0.85^{+0.10}_{-0.09}$	1.000	0.80
841	48.495991	−1.010015	0.2991 ± 0.0005	$-0.17^{+0.16}_{-0.18}$	$1.02^{+0.20}_{-0.16}$	1.000	0.99
1415	6.106480	+0.599307	0.2119 ± 0.0002	$0.66^{+0.13}_{-0.13}$	$0.76^{+0.09}_{-0.08}$	1.000	0.93
1461	24.372675	+0.209735	0.3407 ± 0.0005	$0.33^{+0.11}_{-0.11}$	$1.08^{+0.12}_{-0.12}$	1.000	1.07
1595	−38.432114	−0.554060	0.2136 ± 0.0005	$0.07^{+0.09}_{-0.09}$	$1.03^{+0.08}_{-0.08}$	1.000	1.56
1748	−6.887835	−0.482495	0.3397 ± 0.0001	$0.52^{+0.20}_{-0.19}$	$0.83^{+0.16}_{-0.13}$	0.996	1.00
1775	−41.006622	−1.009430	0.3050 ± 0.0100	$-0.27^{+0.17}_{-0.17}$	$1.26^{+0.15}_{-0.15}$	1.000	1.07
1835	−47.335869	+1.071860	0.2716 ± 0.0100	$-0.19^{+0.19}_{-0.19}$	$1.28^{+0.22}_{-0.20}$	1.000	1.31
...							

Notes.
[a] Internal SN candidate designation.
[b] Coordinates are J2000. Right ascension is given in decimal degrees defined in the range [−180°, +180°].

(This table is available in its entirety in a machine-readable form in the online journal. A portion is shown here for guidance regarding its form and content.)

Table 4
SDSS-II Photo–Ia Candidates

SDSS ID[a]	R.A.[b]	Decl.[b]	$z_{\rm lc}$	A_V	Δm_{15} (B)	$P_{\rm Ia}$	χ^2_r
822	40.560776	−0.862157	$0.167^{+0.065}_{-0.050}$	$0.51^{+0.40}_{-0.47}$	$1.24^{+0.14}_{-0.14}$	1.000	1.38
859	−9.448275	+0.386555	$0.305^{+0.025}_{-0.036}$	$0.04^{+0.28}_{-0.31}$	$0.77^{+0.13}_{-0.09}$	1.000	1.25
904	21.095400	−0.124883	$0.288^{+0.029}_{-0.026}$	$-0.26^{+0.28}_{-0.34}$	$1.10^{+0.22}_{-0.17}$	0.999	1.00
1158	17.275431	−0.352185	$0.694^{+0.006}_{-0.063}$	$-0.58^{+0.50}_{-0.31}$	$1.55^{+0.19}_{-0.29}$	1.000	1.01
1243	−18.340113	−0.764753	$0.188^{+0.100}_{-0.102}$	$0.89^{+0.73}_{-0.67}$	$0.69^{+0.09}_{-0.06}$	1.000	1.47
1285	−38.216843	+0.543195	$0.345^{+0.049}_{-0.078}$	$0.21^{+0.47}_{-0.38}$	$1.06^{+0.25}_{-0.20}$	1.000	1.01
1302	53.654808	+0.891903	$0.282^{+0.039}_{-0.042}$	$-0.10^{+0.26}_{-0.34}$	$0.82^{+0.08}_{-0.08}$	1.000	1.23
1342	−13.472480	+0.117010	$0.299^{+0.046}_{-0.050}$	$0.03^{+0.28}_{-0.31}$	$1.18^{+0.15}_{-0.14}$	1.000	0.90
1354	−5.197145	+0.089970	$0.283^{+0.046}_{-0.056}$	$0.30^{+0.45}_{-0.55}$	$1.50^{+0.20}_{-0.27}$	0.999	0.91
...							

Notes.
[a] Internal SN candidate designation.
[b] Coordinates are J2000. Right ascension is given in decimal degrees defined in the range [−180°, +180°].

(This table is available in its entirety in a machine-readable form in the online journal. A portion is shown here for guidance regarding its form and content.)

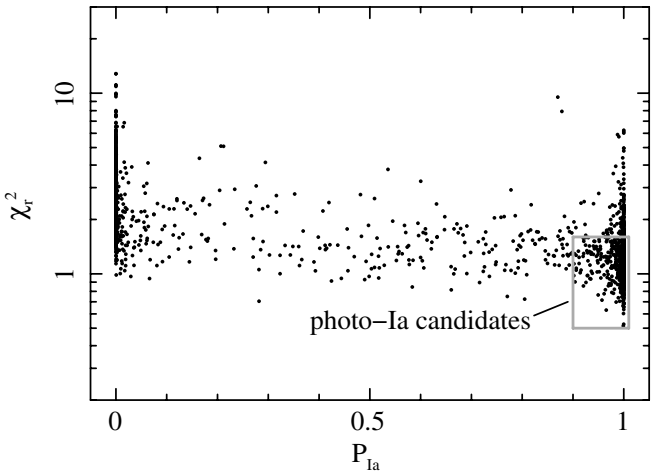

Figure 16. $P_{\rm Ia}$ vs. χ^2_r for the 2776 photometric candidates with no spectroscopic information. The 860 photometric SN Ia candidates are bounded by the gray box shown in the lower right.

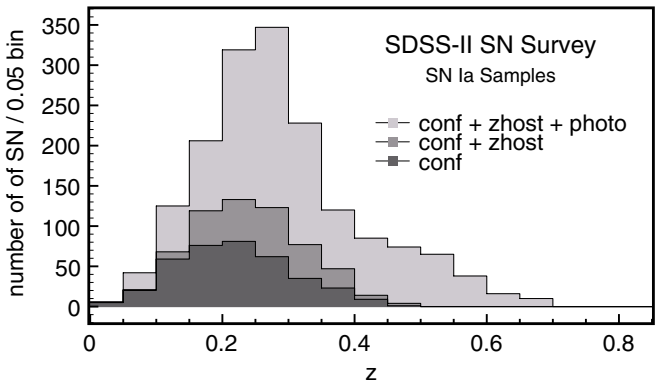

Figure 17. Redshift distributions of the three SN Ia samples.

We compare the spectroscopic redshifts $z_{\rm spec}$ with $z_{\rm lc}$ for the conf-Ia and $z_{\rm host}$-Ia samples and with the host galaxy photometric redshifts $z_{\rm photo}$ from Oyaizu et al. (2008) available

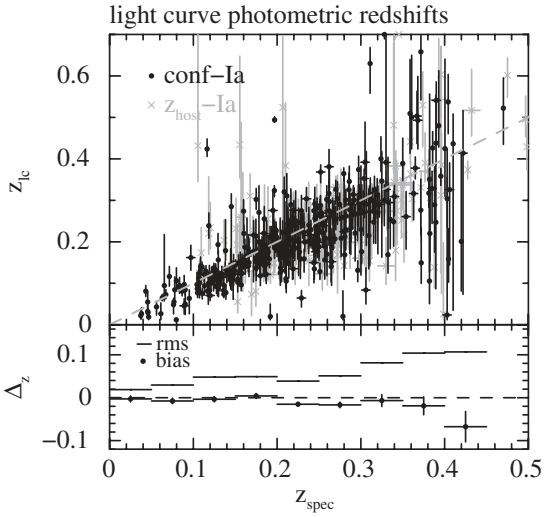

Figure 18. Comparisons of $z_{\rm spec}$ and $z_{\rm lc}$ with a flat redshift prior for the spectroscopic SN Ia sample. The 387 SNe Ia that pass the light curve quality cuts are shown in black while the 210 $z_{\rm host}$-Ia are indicated by gray crosses in the top panel. The bottom panel shows the mean $\Delta_z = (z_{\rm lc} - z_{\rm spec})/(1 + z_{\rm spec})$ values in black circles and the rms as horizontal bars in bins of 0.05 for the combined SN Ia + $z_{\rm host}$-Ia samples. The magnitude of the bias $|\Delta_z|$ is less than 0.02 for $z < 0.4$.

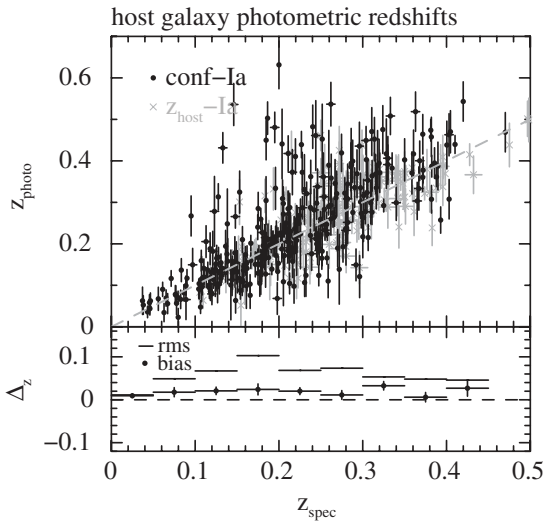

Figure 19. Comparisons of $z_{\rm spec}$ and $z_{\rm photo}$, the photometric redshift of the SN Ia host galaxies from Oyaizu et al. (2008). There are fewer points here than in Figure 18 because there are many SNe Ia with hosts that are below the detection limit of SDSS, and some galaxies are classfied as stars and therefore do not have $z_{\rm photo}$ values. The bottom panel shows the mean Δ_z values in black circles and the rms as horizontal bars in bins of 0.05.

in the SDSS Data Release 8 database. As shown in Figure 18, $z_{\rm lc}$ and $z_{\rm spec}$ are in agreement with $|\Delta_z| < 0.02$ ($\Delta_z \equiv (z_{\rm lc} - z_{\rm spec})/(1 + z_{\rm spec})$) for $z_{\rm spec} < 0.4$, but with a small redshift-dependent bias. The rms scatter is $\Delta_{z,\rm RMS} = 0.05$ below $z_{\rm spec} = 0.30$ and increases to 0.1 at $z = 0.4$.

The sign and magnitude to this bias are similar to those found by Kessler et al. (2010a), who analyzed a subset of the higher S/N SDSS-II SN Ia light curves presented here using both MLCS and SALT-II. Interestingly, a similar bias is seen in their simulations. Rodney & Tonry (2010a) do not quote a value for the bias, but they state that a line with a slope of unity fits the $z_{\rm spec}$ versus $z_{\rm lc}$ values for the first-year SDSS-II SN Ia sample with a $\chi^2_r = 0.98$.

We also show in Figure 19 a comparison of $z_{\rm spec}$ with the host galaxy photometric redshift $z_{\rm photo}$ from Oyaizu et al. (2008). Here, there is a nearly constant bias of $\Delta_z \sim 0.03$ with an rms scatter of $\Delta_{z,\rm RMS} \sim 0.05$–$0.10$.

We show in Figure 20 the Hubble diagram of the 350 conf-Ia, 210 $z_{\rm host}$-Ia, and 860 photo-Ia samples. Distance modulus residuals of the conf-Ia and $z_{\rm host}$-Ia samples relative to a simple quadratic fit are shown in Figure 21. For the conf-Ia sample, the scatter around the mean Hubble relation is $\sigma_\mu = 0.13$ mag at $z = 0.1$ and increases monotonically to $\sigma_\mu = 0.30$ mag at $z = 0.4$. The same Hubble relation was subtracted from the $z_{\rm host}$-Ia sample, which is shown in the bottom panel of Figure 21. There is a noticeably larger scatter with $\sigma_\mu = 0.2$–0.4 mag in the same redshift range. This is most likely due to contamination from non-Ia events, which we have estimated to be at the level of ~6% (approximately 1 out of 16 events in this sample is likely to be a CC SN). The slight deviation of the mean from zero is not statistically significant.

The Hubble diagram of the photo-Ia sample shows extreme outliers below $z \sim 0.1$. All of these points are significantly above the ΛCDM Hubble relation and are most likely CC SNe that are misclassified as SNe Ia. In fact, the majority of these events are classified by PSNID as extremely underluminous, high-extinction ($A_V \gtrsim 1$) SNe Ia. Since the underlying extinction distribution of SN Ia follows the relation $\propto e^{-A_V/\tau_V}$ with $\tau_V \sim 0.33$ (Kessler et al. 2009a) and given the smaller number of confirmed SNe Ia in the same redshift interval, it is unlikely that all of these outlier events are underluminous, high-extinction SNe Ia. Selecting only the candidates with $A_V < 1$ eliminates most of these outliers at the cost of a somewhat reduced efficiency, but measurements of their host galaxy redshifts will also significantly help distinguish their types.

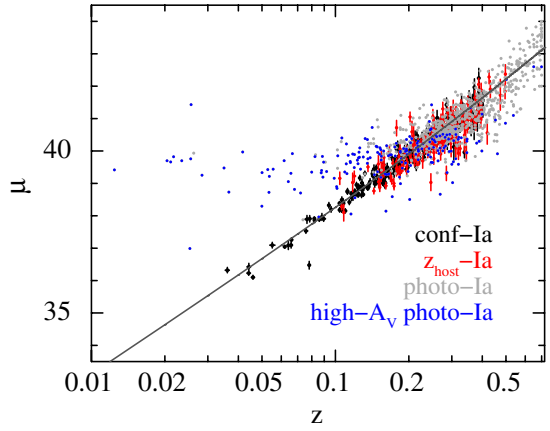

Figure 20. Hubble diagram of the three SN Ia samples (conf-Ia in black, $z_{\rm host}$-Ia in red, and photo-Ia in light gray and blue in the online color version). The dark gray line represents ΛCDM. Spectroscopic redshift priors are used for the conf-Ia and $z_{\rm host}$-Ia samples. Flat redshifts priors are used for the photo-Ia sample. The redshift and distance of the photo-Ia are significantly correlated and their uncertainties are not shown for clarity. The outliers at low-z are probably due to CC SNe that are misclassified as high-A_V ($A_V > 1$) SNe Ia, which are shown in blue. Note that the majority of these points are significantly away from the ΛCDM Hubble relation.

(A color version of this figure is available in the online journal.)

At higher redshifts, the mean Hubble relation of the photo-Ia sample is consistent with the conf-Ia and $z_{\rm host}$-Ia samples, but with a significantly larger scatter. Above $z \sim 0.2$, the rms scatter is $\sigma_\mu \sim 0.5$–0.7 mag, which is a factor of ~2 larger than the scatter in the conf-Ia and $z_{\rm host}$-Ia samples in the same redshift range.

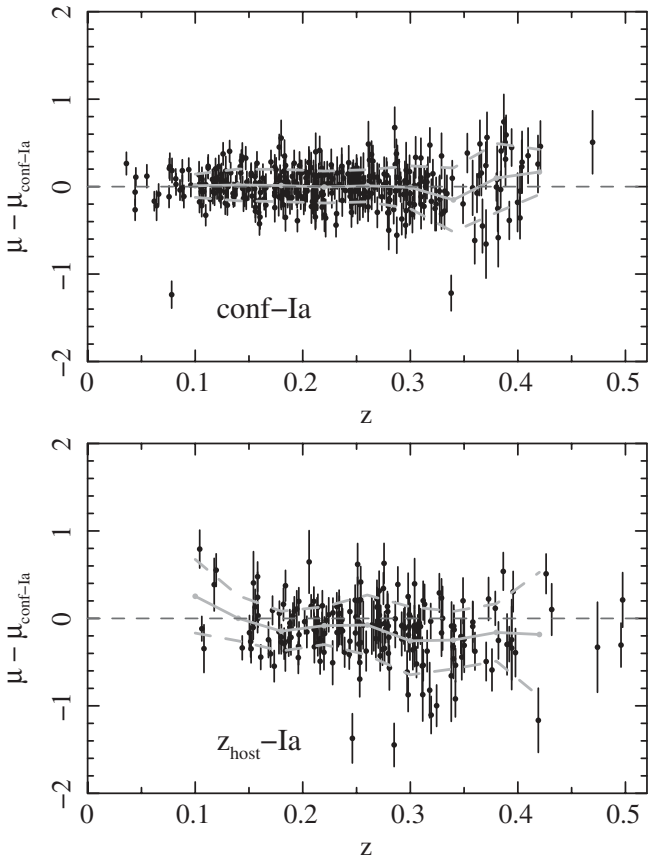

Figure 21. Top: the Hubble residuals of the conf-Ia sample relative to a simple quadratic Hubble relation. The solid line represents the mean residual and the dashed lines represent upper and lower rms values relative to the mean. The scatter ranges from $\sigma_\mu \sim 0.13$ mag to $\sigma_\mu \sim 0.30$ mag in the redshift interval $0.1 < z < 0.4$. Bottom: same except for the $z_{\rm host}$-Ia sample. The same quadratic has been subtracted from the measured distance modulus. The scatter here is larger and ranges from $\sigma_\mu \sim 0.2$ mag to $\sigma_\mu \sim 0.4$ mag in the same redshift range. There is also a small redshift-dependent offset.

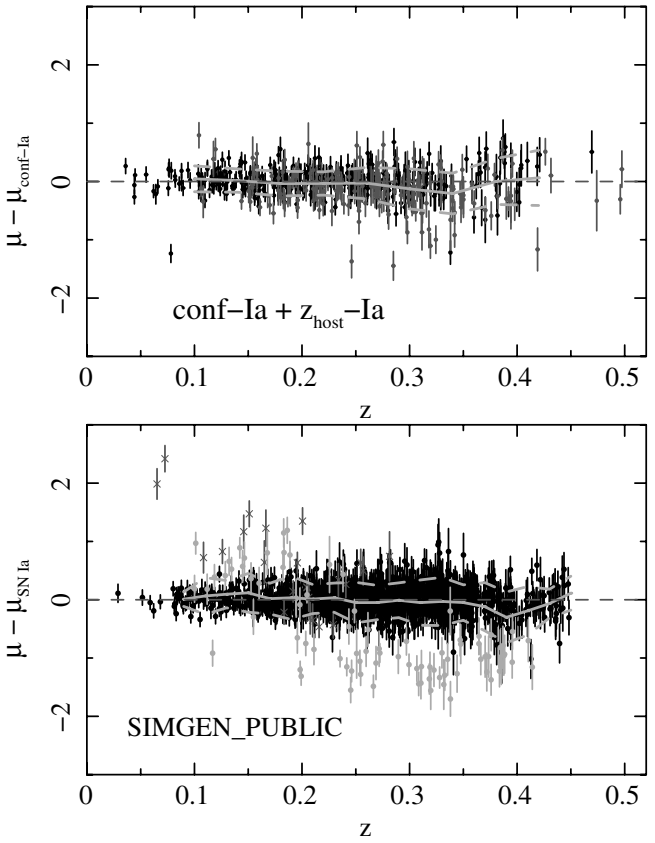

Figure 22. Top: same as in Figure 21 for the combined conf-Ia + $z_{\rm host}$-Ia sample, which are labeled in black and light gray, respectively. The same quadratic function $\mu_{\rm conf-Ia}(z)$ has been subtracted from the measured distance modulus. The rms scatter is slightly larger than that of the conf-Ia sample only. Bottom: simulated SDSS-II SN from K10b. The black, light gray, and dark gray points represent SNe Ia, SN II, and SNe Ib/c, respectively, which pass all of the photometric SN Ia cuts ($P_{\rm Ia} \geqslant 0.9$ and $\chi^2_{z,r} < 1.0$). The residuals shown are relative to a quadratic fit to the simulated SN Ia sample only, whereas the rms scatter shown is for the full sample. Note the slight redshift-dependent bias relative to the SN Ia mean.

7. COMPARISONS WITH SIMULATIONS

The Hubble diagram for the combined conf-Ia + $z_{\rm host}$-Ia sample is shown in the top panel of Figure 22. The scatter is $\sigma_\mu = 0.2$ mag at $z = 0.1$ and increases to $\sigma_\mu = 0.4$ mag at $z = 0.4$, which is slightly larger than the scatter of the conf-Ia sample.

This degradation is probably due to contamination by CC SN events, but to test this hypothesis, we analyzed the sample of simulated SDSS-II SN from K10b. This simulation corresponds to 10 three-season search campaigns, and uses the actual seeing, photometric zero points, and weather from our observing seasons. The bottom panel in Figure 22 shows the Hubble diagram using all events that pass the same light curve quality cuts as well as identical selection criteria in $P_{z,\rm Ia}$–$\chi^2_{z,r}$ space. Specifically, we select SN Ia candidates using $P_{z,\rm Ia} \geqslant 0.9$ and $\chi^2_{z,r} < 1.0$, which is approximately where the efficiency and purity are equal at ∼0.90 for this simulation. The efficiency, purity, and figure-of-merit curves are shown in Figure 23. The average S/N of the $z_{\rm host}$-Ia sample is higher than that of the simulations, so we require in the simulations S/N > 7 in at least two of the *gri* bands. The purity of 90% for this selection is slightly lower than the estimated purity of the $z_{\rm host}$-Ia sample.

The SN Ia Hubble diagram was fitted to a quadratic function and the Hubble residuals of all candidates classified as SNe Ia are shown in the bottom panel of Figure 22. Here, the CC SN

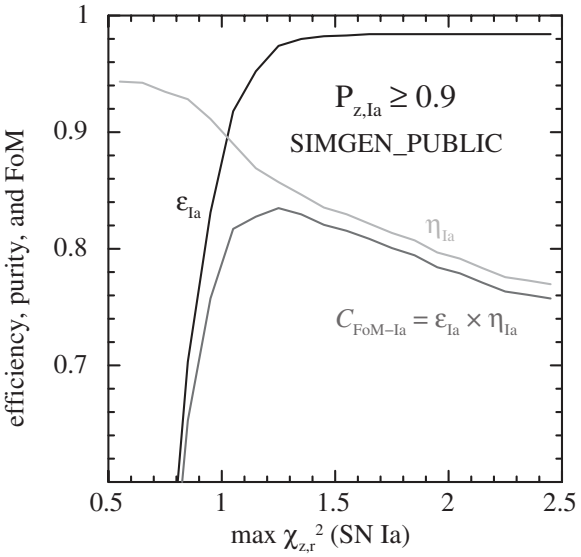

Figure 23. Same as in Figure 10 for simulated SDSS-II SN from K10b except with an additional constraint of S/N > 7 in two bands to approximately match the $z_{\rm host}$-Ia sample.

events are shown in dark (SN Ib/c) and light gray (SN II) points. These false positives are adding scatter and a small redshift-

dependent systematic shift relative to the SN Ia distances, which are represented by black points. The Hubble scatter around the mean for this simulation is $\sigma_\mu = 0.2$–0.4 mag, which is similar to the that of the $z_{\rm host}$-Ia sample over the entire redshift range. The larger scatter seen in the conf-Ia + $z_{\rm host}$-Ia sample is, therefore, most likely due to misclassified CC SNe as reproduced in these simulations.

This set of simulated SDSS-II SN also includes a spectroscopic SN Ia sample selected based on our spectroscopic follow-up strategies and represents our conf-Ia. The Hubble residual scatter of this spectroscopic sample ranges from $\sigma_\mu \sim 0.13$ mag to $\sigma_\mu \sim 0.30$ mag in the redshift interval $0.1 < z < 0.4$, which is nearly identical to the observed scatter of the conf-Ia sample.

8. SUMMARY AND CONCLUSIONS

We have identified 1070 photometric SN Ia candidates from the SDSS-II SN Survey data. This sample is more than three times larger than the spectroscopically confirmed SN Ia sample with good light curves and is estimated to include ∼91% of all SN Ia candidates detected by the survey with a purity of ∼94% (∼6% contamination). This estimate of the purity, however, is based on a limited number of spectroscopically confirmed CC SNe, most of which are nearby, bright events and are therefore not representative of the majority of the contaminating events. As shown in Figure 6, the majority of our photometric candidates have peak r-band S/N < 10, where we have only a handful of spectroscopic SN candidates. To obtain a better characterization of the contaminating sources, confirmation is needed for a much larger sample of faint CC SNe that are comparable in apparent brightness to the photo-Ia sample. As also advocated by Richards et al. (2011), future surveys that rely on photometric identification should obtain spectra of SN candidates over the full range of the S/N of the photometric candidates of interest.

The Hubble diagram with photometric classification and host galaxy spectroscopic redshift priors show a slight increase in scatter over the confirmed SN Ia sample, which is consistent with them being due to misclassified CC SNe. There is no significant redshift-dependent offset in the derived distances compared to the conf-Ia sample. Simulations confirm these findings.

Photometric redshifts estimated from the multiband light curves are unbiased below $z \sim 0.2$ with an rms dispersion of $\sigma_z \sim 0.05$. There is a redshift-dependent bias above $z \sim 0.2$ where the mean redshift difference $\langle z_{\rm lc} - z_{\rm photo} \rangle$ is between -0.04 and -0.02. The rms dispersion is $\sigma_z \sim 0.05$–0.10. The Hubble diagram of the photo-Ia sample also exhibits outliers and redshift-dependent biases. Although the distance and redshift accuracies at present are not yet sufficient for cosmology, the large sample can still be used for studies of the SN Ia rate as a function of redshift, correlations between SN light curves and host galaxy properties, and other studies that do not involve joint constraints on both redshift and distance.

We conclude that cosmology with future large-scale SN surveys should at a minimum measure host galaxy spectroscopic redshifts for the Hubble diagram. A subset of the SN candidates must be observed spectroscopically to study the photometric classification efficiency and purity. Spectroscopy should target candidates with S/N down to the magnitude limit where photometric classification is expected to work. Cosmology with photometry alone, however, requires further investigation with realistic simulations in order to understand and characterize their systematic biases and uncertainties, and how they depend on the SN Ia candidate selection criteria.

We thank the anonymous referee who has helped improve the presentation of the paper. Funding for the SDSS and SDSS-II has been provided by the Alfred P. Sloan Foundation, the Participating Institutions, the National Science Foundation, the U.S. Department of Energy, the National Aeronautics and Space Administration, the Japanese Monbukagakusho, the Max Planck Society, and the Higher Education Funding Council for England. The SDSS Web site is http://www.sdss.org/9.

The SDSS is managed by the Astrophysical Research Consortium for the Participating Institutions. The Participating Institutions are the American Museum of Natural History, Astrophysical Institute Potsdam, University of Basel, Cambridge University, Case Western Reserve University, University of Chicago, Drexel University, Fermilab, the Institute for Advanced Study, the Japan Participation Group, Johns Hopkins University, the Joint Institute for Nuclear Astrophysics, the Kavli Institute for Particle Astrophysics and Cosmology, the Korean Scientist Group, the Chinese Academy of Sciences (LAMOST), Los Alamos National Laboratory, the Max-Planck-Institute for Astronomy (MPIA), the Max-Planck-Institute for Astrophysics (MPA), New Mexico State University, Ohio State University, University of Pittsburgh, University of Portsmouth, Princeton University, the United States Naval Observatory, and the University of Washington.

The Hobby-Eberly Telescope (HET) is a joint project of the University of Texas at Austin, the Pennsylvania State University, Stanford University, Ludwig-Maximillians-Universität München, and Georg-August-Universität Göttingen. The HET is named in honor of its principal benefactors, William P. Hobby and Robert E. Eberly. The Marcario Low-Resolution Spectrograph is named for Mike Marcario of High Lonesome Optics, who fabricated several optics for the instrument but died before its completion; it is a joint project of the Hobby-Eberly Telescope partnership and the Instituto de Astronomía de la Universidad Nacional Autónoma de México. The Apache Point Observatory 3.5 m telescope is owned and operated by the Astrophysical Research Consortium. We thank the observatory director, Suzanne Hawley, and site manager, Bruce Gillespie, for their support of this project. The Subaru Telescope is operated by the National Astronomical Observatory of Japan. The William Herschel Telescope is operated by the Isaac Newton Group, and the Nordic Optical Telescope is operated jointly by Denmark, Finland, Iceland, Norway, and Sweden, both on the island of La Palma in the Spanish Observatorio del Roque de los Muchachos of the Instituto de Astrofisica de Canarias. Observations at the ESO New Technology Telescope at La Silla Observatory were made under programme IDs 77.A-0437, 78.A-0325, and 79.A-0715. Kitt Peak National Observatory, National Optical Astronomy Observatory, is operated by the Association of Universities for Research in Astronomy, Inc. (AURA) under cooperative agreement with the National Science Foundation. The WIYN Observatory is a joint facility of the University of Wisconsin-Madison, Indiana University, Yale University, and the National Optical Astronomy Observatories. The W.M. Keck Observatory is operated as a scientific partnership among the California Institute of Technology, the University of California, and the National Aeronautics and Space Administration. The Observatory was made possible by the generous financial support of the W.M. Keck Foundation. The South African Large Telescope of the South African Astronomical Observatory is operated by a partnership between the National Research Foundation of South Africa, Nicolaus Copernicus Astronomical Center of the Polish Academy of Sciences, the Hobby-

Eberly Telescope Board, Rutgers University, Georg-August-Universität Göttingen, University of Wisconsin-Madison, University of Canterbury, University of North Carolina-Chapel Hill, Dartmouth College, Carnegie Mellon University, and the United Kingdom SALT consortium. The Telescopio Nazionale Galileo (TNG) is operated by the Fundación Galileo Galilei of the Italian INAF Istituo Nazionale di Astrofisica) on the island of La Palma in the Spanish Observatorio del Roque de los Muchachos of the Instituto de Astrofísica de Canarias.

REFERENCES

Abazajian, K. N., Adelman-McCarthy, J. K., Ageros, M. A., et al. 2009, ApJS, 182, 543
Aldering, G., Antilogus, P., Bailey, S., et al. 2006, ApJ, 650, 510
Astier, P., Guy, J., Regnault, N., et al. 2006, A&A, 447, 31
Bailey, S., Aldering, G., Antilogus, P., et al. 2009, A&A, 500, L17
Barris, B. J., & Tonry, J. L. 2004, ApJ, 613, L21
Cardelli, J. A., Clayton, G. C., & Mathis, J. S. 1989, ApJ, 345, 245
Conley, A., Guy, J., Sullivan, M., et al. 2011, ApJS, 192, 1
Contreras, C., Hamuy, M., Phillips, M. M., et al. 2010, AJ, 139, 519
D'Andrea, C. B., Sako, M., Dilday, B., et al. 2010, ApJ, 708, 661
Dahlen, T., Strolger, L.-G., & Riess, A. G. 2008, ApJ, 681, 462
Dahlen, T., Strolger, L.-G., Riess, A. G., et al. 2004, ApJ, 613, 189
Dawson, K. S., Aldering, G., Amanullah, R., et al. 2009, AJ, 138, 1271
Dilday, B., Kessler, R., Frieman, J. A., et al. 2008, ApJ, 682, 262
Dilday, B., Smith, M., Bassett, B., et al. 2010, ApJ, 713, 1026
Eisenstein, D. J., Annis, J., Gunn, J. E., et al. 2001, AJ, 122, 2267
Filippenko, A. V., Li, W. D., Treffers, R. R., & Modjaz, M. 2001, in ASP Conf. Ser. 246, IAU Colloq. 183, Small Telescope Astronomy on Global Scales, ed. W.-P. Chen, C. Lemme, & B. Paczynski (San Francisco, CA: ASP), 121
Flaugher, B. L., Abbott, T. M. C., Annis, J., et al. 2010, Proc. SPIE, 7735, 77350D
Folatelli, G., Phillips, M. M., Burns, C. R., et al. 2010, AJ, 139, 120
Freedman, W. L., Burns, C. R., Phillips, M. M., et al. 2009, ApJ, 704, 1036
Frieman, J., Bassett, B., Becker, A., et al. 2008, AJ, 135, 338
Fukugita, M., Ichikawa, T., Gunn, J. E., et al. 1996, AJ, 111, 1748
Ganeshalingam, M., Li, W., Filippenko, A. V., Anderson, C., et al. 2010, ApJS, 190, 418
Gong, Y., Cooray, A., & Chen, X. 2010, ApJ, 709, 1420
Graur, O., Poznanski, D., Maoz, D., et al. 2011, MNRAS, in press (arXiv:1102.0005)
Gunn, J. E., Carr, M., Rockosi, C., et al. 1998, AJ, 116, 3040
Gunn, J. E., Siegmund, W. A., Mannery, E. J., et al. 2006, AJ, 131, 2332
Guy, J., Sullivan, M., Conley, A., et al. 2010, A&A, 523, A7
Hamuy, M., Phillips, M. M., Suntzeff, N. B., et al. 1996, AJ, 112, 2391
Hicken, M., Wood-Vasey, W. M., Blondin, S., et al. 2009, ApJ, 700, 1097
Holtzman, J., Marriner, J., Kessler, R., et al. 2008, AJ, 136, 2306
Jha, S., Branch, D., Chornock, R., et al. 2006a, AJ, 132, 189
Jha, S., Kirshner, R. P., Challis, P., et al. 2006b, AJ, 131, 527
Johnson, B. D., & Crotts, A. P. S. 2006, AJ, 132, 756
Kessler, R., Bassett, B., Belov, P., et al. 2010a, PASP, 122, 1415
Kessler, R., Becker, A. C., Cinabro, D., et al. 2009a, ApJS, 185, 32
Kessler, R., Bernstein, J. P., Cinabro, D., et al. 2009b, PASP, 121, 1028
Kessler, R., Cinabro, D., Bassett, B., et al. 2010b, ApJ, 717, 40
Kim, A. G., & Miquel, R. 2007, Astropart. Phys., 28, 448
Kunz, M., Bassett, B. A., & Hlozek, R. A. 2007, Phys. Rev. D, 75, 103508
Kuznetsova, N. V., & Connolly, B. M. 2007, ApJ, 659, 530
Lampeitl, H., Nichol, R. C., Seo, H.-J., et al. 2010, MNRAS, 401, 2331
Law, N. M., Kulkarni, S. R., Dekany, R. G., et al. 2009, PASP, 121, 1395
Li, W., Filippenko, A. V., Chornock, R., et al. 2003, PASP, 115, 453
LSST Science Collaborations 2009, arXiv:0912.0201
Matheson, T., Kirshner, R. P., Challis, P., et al. 2008, AJ, 135, 1598
McClelland, C. M., Garnavich, P. M., Galbany, L., et al. 2010, ApJ, 720, 704
Miknaitis, G., Pignata, G., Rest, A., et al. 2007, ApJ, 666, 674
Nugent, P., Kim, A., & Perlmutter, S. 2002, PASP, 114, 803
Oyaizu, H., Lima, M., Cunha, C. E., et al. 2008, ApJ, 674, 768
Palanque-Delabrouille, N., Ruhlmann-Kleider, V., Pascal, S., et al. 2010, A&A, 514, A63
Panagia, N. 2003, in Supernovae and Gamma-Ray Bursters, ed. K. Weiler (Lecture Notes in Physics; Vol. 598; Berlin: Springer), 113
Perlmutter, S., Aldering, G., Goldhaber, G., et al. 1999, ApJ, 517, 565
Phillips, M. M. 1993, ApJ, 413, L105
Phillips, M. M., Li, W., Frieman, J. A., et al. 2007, PASP, 119, 360
Phillips, M. M., Lira, P., & Suntzeff, N. B. 1999, AJ, 118, 1766
Poznanski, D., Gal-Yam, A., Maoz, D., et al. 2002, PASP, 114, 833
Poznanski, D., Maoz, D., & Gal-Yam, A. 2007a, AJ, 134, 1285
Poznanski, D., Maoz, D., Yasuda, N., et al. 2007b, MNRAS, 382, 1169
Prieto, J. L., Garnavich, P. M., Phillips, M. M., et al. 2007, arXiv:0706.4088
Pskovskii, I. P. 1977, Sov. Astron. Lett., 3, 215
Rau, A., Kulkarni, S. R., Law, N. M., et al. 2009, PASP, 121, 1334
Richards, G. T., Fan, X, Newberg, H. Jo, et al. 2002, AJ, 123, 2945
Richards, J. W., Homrighausen, D., Freeman, P. E., Schafer, C. M., & Poznanski, D. 2011, MNRAS, submitted (arXiv:1103.6034)
Riess, A. G., Filippenko, A. V., Challis, P., et al. 1998, AJ, 116, 1009
Riess, A. G., Kirshner, R. P., Schmidt, B. P., et al. 1999, AJ, 117, 707
Riess, A. G., Strolger, L-G., Casertano, S., et al. 2007, ApJ, 659, 98
Riess, A. G., Strolger, L-G., Tonry, J., et al. 2004a, ApJ, 607, 665
Riess, A. G., Strolger, L-G., Tonry, J., et al. 2004b, ApJ, 600, L163
Rodney, S. A., & Tonry, J. L. 2009, ApJ, 707, 1064
Rodney, S. A., & Tonry, J. L. 2010a, ApJ, 715, 323
Rodney, S. A., & Tonry, J. L. 2010b, ApJ, 723, 47
Sako, M., Bassett, B., Becker, A., et al. 2008, AJ, 135, 348
Schneider, D. P., Richards, G. T., Hall, P. B., et al. 2010, AJ, 139, 2360
Scolnic, D. M., Riess, A. G., Huber, M. E., et al. 2009, ApJ, 706, 94
Sollerman, J., Mrtsell, E., Davis, T. M., et al. 2009, ApJ, 703, 1374
Strauss, M. A., Weinberg, D. H., Lupton, R. H., et al. 2002, AJ, 124, 1810
Sullivan, M., Howell, D. A., Perrett, K., et al. 2006, AJ, 131, 960
Wang, Y. 2007, ApJ, 654, L123
Wang, Y., Narayan, G., & Wood-Vasey, M. 2007, MNRAS, 382, 377
Wood-Vasey, W. M., Miknaitis, G., Stubbs, C. W., et al. 2007, ApJ, 666, 694
York, D. G., Adelman, J., Anderson, J. E., Jr., et al. 2000, AJ, 120, 1579
Zheng, C., Romani, R. W., Sako, M., et al. 2008, AJ, 135, 1766